Effect of Time Dependence on Probabilistic Seismic-Hazard Maps and Deaggregation for the Central Apennines, Italy

Article *in* Bulletin of the Seismological Society of America · April 2009

DOI: 10.1785/0120080053

CITATIONS
119

READS
431

6 authors, including:

Aybige Akinci
National Institute of Geophysics and Volcanology
152 PUBLICATIONS **3,127** CITATIONS
SEE PROFILE

Fabrizio Galadini
National Institute of Geophysics and Volcanology
239 PUBLICATIONS **6,515** CITATIONS
SEE PROFILE

D. Pantosti
National Institute of Geophysics and Volcanology
247 PUBLICATIONS **6,670** CITATIONS
SEE PROFILE

Mark D. Petersen
United States Geological Survey
139 PUBLICATIONS **5,647** CITATIONS
SEE PROFILE

Bulletin of the Seismological Society of America, Vol. 99, No. 2A, pp. 585–610, April 2009, doi: 10.1785/0120080053

Effect of Time Dependence on Probabilistic Seismic-Hazard Maps and Deaggregation for the Central Apennines, Italy

by A. Akinci, F. Galadini, D. Pantosti, M. Petersen, L. Malagnini, and D. Perkins

Abstract We produce probabilistic seismic-hazard assessments for the central Apennines, Italy, using time-dependent models that are characterized using a Brownian passage time recurrence model. Using aperiodicity parameters, α of 0.3, 0.5, and 0.7, we examine the sensitivity of the probabilistic ground motion and its deaggregation to these parameters. For the seismic source model we incorporate both smoothed historical seismicity over the area and geological information on faults. We use the maximum magnitude model for the fault sources together with a uniform probability of rupture along the fault (floating fault model) to model fictitious faults to account for earthquakes that cannot be correlated with known geologic structural segmentation.

We show maps for peak ground acceleration (PGA) and 1.0 Hz spectral acceleration (SA_1) on rock having 10% probability of exceedence in 50 yr. We produce maps to compare the separate contributions of smoothed seismicity and fault components. In addition we construct maps that show sensitivity of the hazard for different α parameters and the Poisson model.

For the Poisson model the addition of fault sources to the smoothed seismicity raises the hazard by 50% at locations where the smoothed seismicity contributes the highest hazard and up to 100% at locations where the hazard from smoothed seismicity is low. For the strongest aperiodicity parameter (smallest α), the hazard may further increase 60%–80% or more or may decrease by as much as 20% depending on the recency of the last event on the fault that dominates the hazard at a given site.

In order to present the most likely earthquake magnitude and/or the most likely source-site distance for scenario studies, we deaggregate the seismic hazard for SA_1 and PGA for two important cities (Rome and L'Aquila). For PGA both locations show the predominance of local sources having magnitudes of about 5.3 and 6.5, respectively. For SA_1 at a site in Rome, there is significant contribution from local smoothed seismicity and an additional contribution from the more distant Apennine faults having magnitude around 6.8. For L'Aquila the predominant sources remain local.

In order to show the variety of impact of different α values, we also obtained deaggregations for another three sites. In general, as α decreases (periodicity increases), the deaggregation indicates that the hazard is highest near faults with the highest earthquakes rates. This effect is strongest for the long-period (1 sec) ground motions.

Introduction

In recent years time-dependent earthquake recurrence models have been an important component of many probabilistic seismic-hazard analyses (PSHA; e.g., Working Group on California Earthquake Probabilities [WGCEP], 1995; Kumamoto, 1999; Cramer *et al.*, 2000; Papaioannou and Papazachos, 2000; Frankel *et al.*, 2002; Peruzza and Pace, 2002; WGCEP, 2003; Erdik *et al.*, 2004; Pace *et al.*, 2006; Petersen *et al.*, 2007, 2008). There has been some debate on the relative merits of Poissonian and nonPoissonian recurrence models for use in building codes and earthquake insurance rates. However, the question of whether the time-dependent models of seismic hazard provide sufficiently important information for public policy applications is still open. The focus of this article is to investigate the differences that these two different recurrence models make in the assessment of earthquake-induced ground-motion hazard. Deaggregations of the hazard indicate the earthquakes (magnitude, distances) that contribute most to the hazard at a site and are used to

help define scenario earthquakes that can be used for public policy planning. Because of the large amount of fault information that has recently become available for the central Apennines, we selected this area as a case study for developing time-dependent hazard models. Historical and recent earthquake sequences in the central Apennines have raised hazard awareness, and this, in turn, has motivated the identification of several active faults and the estimation of seismic rates also for regions that have been silent during historical time (Barchi *et al.*, 2000; Galadini and Galli, 2000; Valensise and Pantosti, 2001).

We compiled geologic data describing the geometry and activity (fault lengths, slip rates [SR], single-event displacements, and return times) for the major active faults and combined these data with the historical seismicity to assess the fault seismicity parameters. In order to express the time dependence of the seismic processes to predict the future ground motions that will occur across the region, we used a Brownian passage time (BPT) model characterized by a mean recurrence, aperiodicity, or uncertainty in the recurrence distribution and elapsed time since the last earthquake (Matthews *et al.*, 2002). Although other parameters such as static elastic fault interactions, visco-elastic stress-transfer, and dynamic stress changes from earthquakes on nearby faults will also influence the probabilities for earthquake occurrence, in our study we consider only the influence of the elapsed time since the last earthquake.

Results for both BPT and Poisson models are presented in terms of maps of PGA and 1.0 sec spectral response acceleration (SA_1) for 10% probability of exceedance in 50 yr. The general strategy used in our study is similar to that used in the preparation of seismic-hazard maps for California, the United States (Petersen *et al.*, 1996, Frankel *et al.*, 2002; Petersen *et al.*, 2008), and for the Marmara Region in Turkey (Erdik *et al.*, 2004).

To determine the relative contribution from various sources at L'Aquila and Rome, we deaggregated the seismic hazard for SA_1 and PGA following the approach described by Harmsen and Frankel (2001). These cities have been selected because they are two of the most densely populated metropolitan areas in the region. They have a high concentration of historical monuments and industrial facilities and high political, economic, and strategic relevance.

Pace *et al.*, 2006 have also developed a PSHA for the same area. However, our study differs from that one in many respects. The first difference is the use of the background seismicity parameters and the seismic catalogs in the hazard calculations. For example, we use historical catalogs, Working Group Catalogo Parametrico dei Terremoti Italiani (CPTI, 2004) and *a* constant *b*-value distribution for the background seismicity hazard while Pace *et al.* (2006) use Catalogo Strumentale dei Terremoti Italiani (CSTI, 2001) instrumental catalogs with spatially variable *b* value. Another difference is the geologic data for the fault sources as well as the earthquake recurrence models. For example, we calculate the seismic hazard for the faults that have magnitudes greater than 5.9 while it is $M > 5.5$ in their study. We associate an elapsed time calculated from 500 A.D. as a conventional date for previous rupture on faults that did not have a historical earthquake and use time-dependent model to calculate the seismic hazard for these faults. Instead, Pace *et al.*, 2006 treated those with the time-independent model. For some specific faults (see following section), we use different magnitudes, SR, and elapsed time parameters. For this reason we provide a considerable amount of detail for our sources in this study. The last difference is time-dependent recurrence parameters from observed-recurrence times. In contrast, Pace *et al.* (2006) derived aperiodicity parameters from the statistics of alternative methods of determining maximum magnitude, M_{max}. We estimated aperiodicity (α values) for three faults where the recurrence intervals were already available and used these values as a guide for selecting the range of α values to be used in our sensitivity analysis. On the contrary, Pace *et al.* (2006) did not attempt a sensitivity analysis on α values.

Active Faults/Seismogenic Sources in the Central Apennines

Seismotectonic Framework

The central Apennines are characterized by extensional tectonics since the Pliocene (e.g., Consiglio Nazionale delle Ricerce [CNR]-Progetto Finalizzato Geodinamica [PFG] 1987; Elter *et al.*, 2003) with most of the active faults showing normal or normal-oblique movement. In this area the main active faults trend northwest–southeast and north-northwest–south-southeast parallel to the general physiographic features of the chain with only a few faults trending west-northwest–east-southeast (Fig. 1).

Faults showing evidence of late Pleistocene–Holocene activity are considered active in this work (e.g., Barchi *et al.*, 2000; Galadini and Galli, 2000; Pantosti and Valensise, 2001). The length of fault sections mapped at the surface ranges between 5 and 20 km, with dips of 40°–60° usually to the west or southwest. These fault sections are frequently organized in dextral stepover systems consisting of 3 to 5 segments. The total length of these stepover fault systems does not exceed 33 km (i.e., Fucino and Gran Sasso fault).

At a regional scale, fault systems and individual faults are organized into larger fault sets that run almost parallel to the Apennine chain axis (Fig. 1). The number of fault sets and their relevance to seismic hazard is still a matter of debate. Boncio *et al.* (2004a) define three fault sets but other regional compilations (e.g., Galadini and Galli, 2000; Valensise and Pantosti, 2001; Basili *et al.*, 2008) or specific fault case studies (e.g., D'Addezio *et al.*, 2001) identify no more than two active fault sets (Fig. 1). The debated set is related to faults located in the western sector of the study area because there is evidence for inactivity or very low activity along these faults (Galadini and Messina, 2004). In this work, we adopted only two main active fault sets (A and B, Fig. 1) and introduced two of the faults (9 and 16) com-

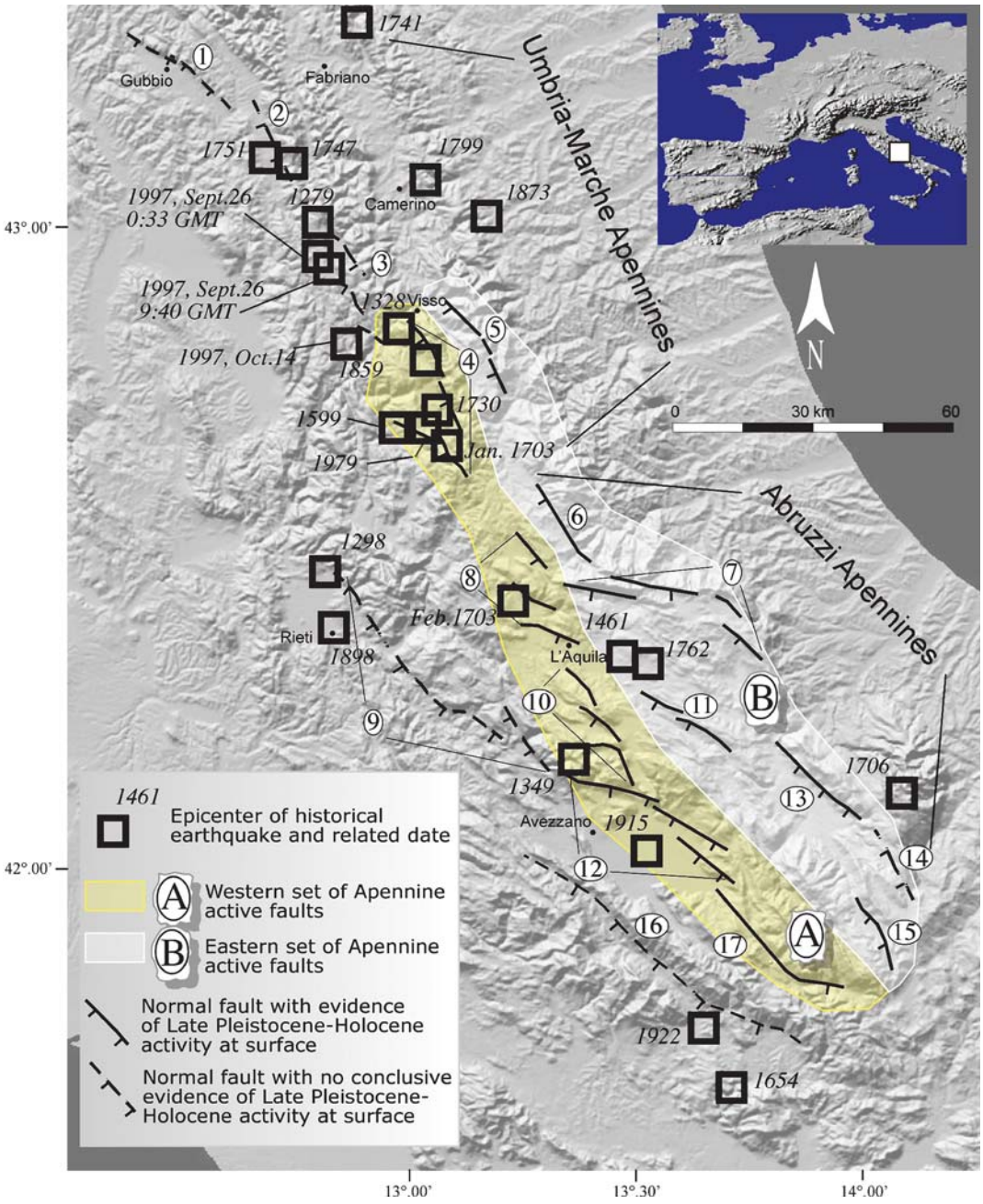

Figure 1. Primary, active faults and $M_w \geq 5.5$ historical earthquakes after Working Group CPTI (2004) in the investigated sector of the central Apennines. Legend: (1) Gubbio fault system, (2) Gualdo Tadino fault, (3) Colfiorito fault system, (4) Norcia fault system, (5) Mt. Vettore fault system, (6) Laga Mts. fault, (7) Campo Imperatore Assergi fault system, (8) L'Aquila, Upper Aterno Valley fault system, (9) Salto Valley fault, (10) Ovindoli–Pezza–Campo Felice fault system, (11) Middle Aterno fault system, (12) Fucino fault system, (13) Mt. Morrone fault system, (14) Maiella, Mt. Porrara fault, (15) Aremogna–Cinquemiglia fault, (16) Liri Valley fault, (17) Upper Sangro fault.

posing the third set of Boncio *et al.* (2004a) as secondary structures with uncertain activity.

The Geometry and Kinematics of Faults in the Apennines

The fault strike, location, length, and SR/recurrence interval derived from surface investigations for the two main active fault sets are considered representative of the seismogenic sources at depth. The geometries and source parameters used in this model are mainly derived from the synthesis provided by Galadini and Galli (2000) and Valensise and Pantosti (2001) integrated with recent geologic mapping (see Table 1) with subsurface information, seismology, and geodesy (e.g., Barchi *et al.*, 2000; Salvi *et al.*, 2000; Lundgren and Stramondo, 2002; Mirabella and Pucci, 2002; Pizzi *et al.*, 2002). Starting from the surficial and subsurficial fault geo-

Table 1
Geometric Parameters of the Fault Segments in the Central Apennines

Number*	Faults	Slip Rates (mm/yr)†	Width (km)	Length (km)	M_w	Depth (km)	Fault Dip (°)
1,2,3,4	Gubbio, G. Tadino, Colfiorito, Norcia (float fault)	0.20	15	139	5.9	8.0	−60
1	Gubbio	0.20	20	22	6.2	8.0	−40
2	Gualdo Tadino	0.20	15	16	6.3	13.0	−60
3	Colfiorito, Sellano	0.20	20	23	6.3	13.0	−40
4	Norcia	0.65	15	42	6.8	13.0	−40
5	Mt. Vettore	0.40	15	22	6.5	13.0	−60
6	Laga Mts. (Campotosto)	0.50	14	29	6.6	13.0	−65
7	Campo Imperatore Assergi	0.50	15	44	6.8	13.0	−65
8	L'Aquila	0.60	15	34	6.7	13.0	−60
9	Martani Mts. South, Salto– Velino Valleys (float fault)	0.10	14	47	6.0	13.0	−70
10	Ovindoli–Pezza	0.65	15	23	6.5	13.0	−60
11	Middle Aterno Valley	0.60	15	21	6.5	13.0	−60
12	Fucino	0.65	17	56	7.0	13.0	−50
13	Mt. Morrone	0.50	15	21	6.5	13.0	−60
14	Maiella	0.60	15	28	6.6	13.0	−60
15	Aremogna–Cinquemiglia	0.50	15	21	6.5	13.0	−60
16	Liri Valley–Sora (float. fault)	0.20	15	62	6.2	13.0	−60
17	Upper Sangro Valley	0.40	17	22	6.5	13.0	−50
18	Poggio Picenze	0.60	13	11	6.0	13.0	−60
19	Fabriano–Camerino (float fault)	0.10	15	51	5.9	13.0	−60

*Data from (1) Pucci *et al.* (2003). (2) Barchi *et al.* (2000). (3) Salvi *et al.* (2000); Lundgren and Stramondo (2002); Messina *et al.* (2002); Mirabella and Pucci (2002); De Martini *et al.* (2003); Chiaraluce *et al.* (2005). (4) Blumetti (1995); Pizzi and Scisciani (2000); Galli *et al.* (2002). (5) Galadini and Galli (2003). (6) Galadini and Galli (2003); Boncio *et al.* (2004b). (7) Carraro and Giardino (1992); Giraudi and Frezzotti (1995); Galadini *et al.* (2003). (8) Galadini and Galli (2000); Moro *et al.* (2002). (9) Barchi *et al.* (2000). (10) Salvi and Nardi (1995); Pantosti *et al.* (1996); Salvi *et al.* (2003). (11) Galadini and Galli (2000). (12) Galadini and Galli (1999); Galadini and Messina (2001); Galli *et al.* (2002). (13) Cavinato and Miccadei (1995); Vittori *et al.* (1995); Gori *et al.* (2007). (14) Gasperini *et al.* (1999). (15) D'Addezio *et al.* (2001). (16) Barchi *et al.* (2000). (17) Galadini and Messina (1993); Galadini *et al.* (1998). (18) This article. (19) Barchi *et al.* (2000).

†Seismic behavior (SR, M_{max}).

metry derived from geological data, the source dimensions (Table 1) have been defined using the magnitude of the earthquake associated with each fault (for the cases defined in Table 2). Therefore, source length and width are consistent with the expected energy release.

Generally, SR have been geologically determined, that is, by means of the displacement affecting dated quaternary deposits and/or landforms or the displacement of late Pleistocene–Holocene stratigraphic units observed in trenches excavated during paleoseismological investigations.

The Northern Sector

Although numerous studies were recently conducted in the study area (e.g., Barchi *et al.*, 2000; Pucci *et al.*, 2003), in the northern sector no conclusive evidence of late Pleistocene–Holocene activity at the surface has been obtained. Moreover, no obvious evidence for recent faulting was recognized in the area east of Gubbio (Fig. 1) even though this area experienced earthquakes with M_w estimated about 6.0 (1741 and 1799; Fig. 1). In such cases, the source parameters for PSHA input (magnitude and source) were derived mainly from the damage distribution of the historical earthquakes through the Boxer algorithm (Gasperini *et al.*, 1999). This algorithm estimates magnitude by the macroseismic intensity reports and then estimates an axis by finding an orientation in which the near-field intensity appears to be elongated. Then, given the magnitude and axis, the algorithm can be used to create a box from which a magnitude can be estimated using length and width derived from empirical relations given by Wells and Coppersmith (1994).

Because of the lack of geological information to directly derive the slip rate for some sources, we assume this can be considered similar to that of nearby sources for which the slip rate is available. For instance, the slip rate for the Colfiorito fault system was defined by integrating 1997 coseismic geodetic slip derived from geodetic and interferometric synthetic aperture radar (InSAR) modeling with historical information. In this case the coseismic slip is better known at depth that is an estimated 20–30 cm (Salvi *et al.*, 2000; Lundgren and Stramondo, 2002; De Martini *et al.*, 2003) and can be translated to 10–20 cm at the surface by using common elastic dislocation models. Assuming that the previous earthquake on the same source occurred in 1279 (Galadini *et al.*, 1999), a mean-recurrence time of 700 yr is hypothesized. These estimates yield a slip rate of ca. 0.15–0.28 mm/yr for the Colfiorito source. For the sake of simplicity we adopt the mean value of 0.2 mm/yr.

On the hypothesis that the Gubbio fault system (Pucci *et al.*, 2003) and Gualdo Tadino structures share a similar tectonic setting and seismogenic behavior with the Colfiorito system, we assumed that the slip rate of this latter system (0.2 mm/yr) is representative also for the Gubbio and Gualdo structures. On the basis of displaced geomorphic fea-

Table 2

Time-Dependent Fault Segments with Their Rates and Probabilities for Poisson and Time-Dependent (BPT) and PSHA Models Together with Their Elapsed Time Ratios[*] and Mean Recurrence Intervals[†]

Number	Faults	Previous Events	Last Events	Recurrence Time, *T*-bar	Poisson Annual Rate	Renewal BPT, $\alpha = 0.5$ 50 yr probabilities	*T*-lapse[‡]	Model
1,2,3,4	Gubbio, G. Tadino, Colfiorito, Norcia	1328, 1599, 1730, 1747, 1859, 1984, 1997, 1979	1997	103	9.71×10^{-3}	1.683×10^{-1}	0.07	Float Fault
1	Gubbio	-	([§])	1348	7.42×10^{-4}	7.36×10^{-2}	1.12	Char. Model
2	Gualdo Tadino	1751	1751	2215	4.51×10^{-4}	1.52×10^{-6}	0.10	Char. Model
3	Colfiorito, Sellano	1279	1279	1160	8.62×10^{-4}	5.84×10^{-2}	0.62	Char. Model
4	Norcia	1703	1703	1458	6.86×10^{-4}	1.21×10^{-3}	0.20	Char. Model
5	Mt. Vettore	-	([§])	1627	6.15×10^{-4}	5.69×10^{-2}	0.92	Char. Model
6	Laga Mts. (Campotosto)	-	([§])	1442	6.93×10^{-4}	6.75×10^{-2}	1.04	Char. Model
7	Campo Imperatore Assergi	-	([§])	1789	5.59×10^{-4}	4.895×10^{-2}	0.84	Char. Model
8	L'Aquila	1703	1703	1369	7.30×10^{-4}	2.04×10^{-3}	0.22	Char. Model
9	Martani Mts. South Salto-Velino Valleys	1298, 1898	1898	573	1.75×10^{-3}	4.29×10^{-3}	0.18	Float Model
10	Ovindoli-Pezza	([#])	1349(?)	941	1.06×10^{-3}	8.0×10^{-2}	0.70	Char. Model
11	Middle Aterno Valley	-	([§])	1132	8.84×10^{-4}	9.14×10^{-2}	1.32	Char. Model
12	Fucino	([‖])	1915	1910	5.24×10^{-4}	4.9×10^{-14}	0.04	Char. Model
13	Mt. Morrone	125	125	1360	7.35×10^{-4}	7.65×10^{-2}	1.38	Char. Model
14	Maiella	1706	1706	1160	8.62×10^{-4}	5.73×10^{-3}	0.47	Char. Model
15	Aremogna-Cinquemiglia	-	([§])	1381	7.24×10^{-4}	7.18×10^{-2}	1.09	Char. Model
16	Liri Valley–Sora	1654, 1922	1922	402	2.49×10^{-3}	1.51×10^{-2}	0.20	Float Fault
17	Upper Sangro Valley	-	([§])	1429	7.0×10^{-4}	6.84×10^{-2}	1.05	Char. Model
18	Poggio Picenze	1461, 1762	1762	405	3.53×10^{-3}	1.62×10^{-1}	0.60	Char. Model
19	Fabrianese	1799, 1873, 1741	1873	343	2.92×10^{-3}	1.06×10^{-1}	0.38	Float Fault

[*] *T*-lapse/*T*-bar

[†] *T*-bar

[‡] Equals lapse time since the last earthquake

[§] We assume activation on 500 A.D. for the Gubbio, Campo Imperatore Assergi, Mt. Vettore, Laga Mts. (Campotosto), Middle Aterno Valley, Mt. Morrone, Sangro, and Aremogna–Cinquemiglia sources deriving from the mean of the time span 0–1000 A.D. (see Galadini and Galli, 2001, 2003; Galadini *et al.*, 2003).

[‖] Paleoseismological earthquakes, 508–618 A.D., 1100–1600 B.C., 2200–3944 B.C., 400–5979 B.C., 5770–10,729 B.C., 10,053–10,729 B.C.

[#] Paleoseismological earthquakes, 1300 A.D.–1690 B.C., 1420–5620 B.C., 5460–20,000 B.P.

tures, a minimum slip rate of 0.2 mm/yr was estimated also for the Norcia fault system (Blumetti, 1995) that is the source of historical $M_w \geq 6$ earthquakes. On the basis of the system length, magnitude of last earthquake (1703, M_w 6.8), a slip rate of 0.65 mm/yr is proposed in the present work (4 in Fig. 1 and Tables 1 and 2). Given the large uncertainty on the seismic behavior of these structures, we also modeled them as a floating rupture along the Gualdo, Gubbio, Colfiorito, and Norcia faults. The slip rate applied to the floating rupture was fixed at 0.2 mm/yr.

A slightly lower slip rate was attributed to the Fabriano–Camerino source (0.10 mm/yr, the minimum considered in this study), which for the reasons given previously, is only modeled as a floating fault.

The Southern Sector

The amount of seismotectonic data increases significantly in the southern part of the target area. In this area most of the faults composing the two parallel active fault sets (Fig. 1) were mapped and characterized using active tectonics, geomorphic, and paleoseismological investigations initiated by Bosi (1975) and further developed during the past 30 yr (see Table 1 for references listed according to fault). For these faults we used the parameters directly obtained in these studies (see Table 1).

In fact, the available data indicate that in the southern sector none of the historical earthquakes that occurred during approximately the past 1000 yr can be associated with the six seismogenic sources of the eastern fault set (i.e., numbers 5, 6, 7, 11, 13, 15 in Fig. 1 and Tables 1 and 2) with only one fault of the western set (number 17 in Fig. 1 and Tables 1 and 2). Thus, in such cases the elapsed time since the last earthquake should exceed 1000 yr for any fault. On the basis of paleoseismological and archaeoseismological data, the average recurrence times in the target area are inferred to be longer than 1000 years (e.g., Pantosti *et al.*, 1996; Galadini

and Galli, 2000; D'Addezio *et al.*, 2001; Galadini and Galli, 2001). Because there is some evidence of large earthquakes for a few of these sources in the preceding millennium, we assume the elapsed times for the sources to be on the order of 1,000–2,000 yr. We set the occurrence of the last earthquake on the sources that have not ruptured during the last 3,000 yr at 500 A.D., and we set the elapsed time at 1500 yr B.P. (Table 2). The choice of 500 A.D. is conventional; it is a fixed date in order to emphasize these faults have not had an earthquake in a long time. When we deal with periods preceding 1000 A.D., knowledge on the historical earthquakes is so sparse that in many cases conventional dates have been attributed to the unknown events caused by well known seismogenic sources.

Conversely, for those faults that are less known we had to infer parameters similarly to the methods used in the northern sector of the target area. These faults (i.e., the two located to the western part of this sector) are considered as potentially responsible for earthquakes with M_w about 6 and are modeled as floating faults. A low slip rate (0.10 mm/yr, the minimum considered in this study) was assumed for the Salto-Rieti fault (number 9 in Fig. 1 and Tables 1 and 2), whereas a 0.20 mm/yr was inferred for the Liri Valley–Sora source (number 16 in Fig. 1 and Tables 1 and 2).

Unresolved Issues and Adopted Choices

Two major unresolved issues are the association of historical damaging earthquakes with faults identified in the area and the probable overestimation of some magnitudes estimated from historical data.

1706 Earthquake. The 1706 M_w 6.6 earthquake (Fig. 1) is located in the southern part of the study. Different hypotheses are available for its association with identified faults (Meletti *et al.*, 1988; Gasperini *et al.*, 1999). Because the seismotectonic framework of the 1706 earthquake area is still unclear, in this work we adopt the magnitude and source size solution derived from the Boxer program (Gasperini *et al.*, 1999) and reported in Valensise and Pantosti (2001, number 14 in Fig. 1 and Tables 1 and 2).

1654 Earthquake. The Sora area (southwest sector of the target area) was struck in 1654 by an M_w 6.2 earthquake (Fig. 1), but no conclusive data are available on the identification of the responsible fault (e.g., Carrara *et al.*, 1995). One possibility is that the earthquake magnitude has been overestimated and/or the event was produced by a blind source. For this reason, we decided to include the 1654 earthquake source in a floating rupture source. (number 16 in Fig. 1 and Tables 1 and 2).

1461 and 1639 Earthquakes. Both the 1461 earthquake and the 1639 earthquake sequences occurred near L'Aquila (see Fig. 1 for the location of the 1461 event, while the 1639 earthquake epicenter [it is not in the map] was located about 30 km north of L'Aquila). Given the limited amount of historical information available and the fact these occurred as earthquake sequences, the revision of their CPTI (2004) magnitudes suggests that these are likely overestimates. For the 1461 event, an M_w 6.5 is attributed by CPTI. However, because it produced significant damage only in a small area of the Middle Aterno Valley and given the general tectonic setting of the area (Bosi and Bertini, 1970; Bertini and Bosi, 1993), we forced the association of the 1461 earthquake seismogenic source to the northwest–southeast Poggio–Picenze structure that is consistent with a M_w 6.0 earthquake (number 18 in Fig. 1 and Tables 1 and 2).

Working Group CPTI (2004) attributes an M_w 6.3 to the 1639 earthquake. However, this earthquake is also likely to be a sequence of events (Camassi and Castelli, 2004). Thus, the CPTI (2004) magnitude is expected to be higher than that of the separate earthquakes. In this case, we consider all of the earthquakes composing the 1639 sequence to be smaller than M_w 5.9, and thus in our PSHA model, to belong to the background seismicity. Therefore, no individual source has been imaged for these earthquakes.

1315 Earthquake. An M_w 6.0 earthquake is reported by Working Group CPTI (2004) in 1315. However, the poor historical information available suggests that both the magnitude and location attributed to this event are too uncertain to associate this event to any defined seismogenic source. For this reason we do not include the 1315 event in our fault model. Therefore, it also belongs to the background seismicity.

PSHA Methodology and Models

We construct a PSHA model for the central Apennines based on the long-term recurrence behavior of active faults together with the spatial distribution of earthquakes observed in historic time. The basic procedure for constructing the hazard maps is shown in Figure 2. The earthquake hazard in the region is assumed to result from the following contributions: (1) The background earthquake model based on seismicity that does not occur on the known faults (Model-1, historical and instrumental earthquake catalogs for events

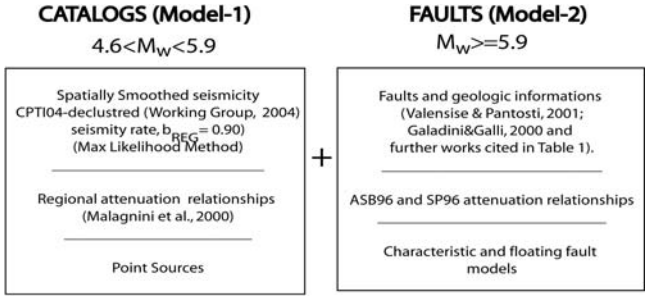

Figure 2. Scheme used to make hazard calculations for the central Apennines.

$4.6 \leq M_w < 5.9$) and (2) The geologic data from individual fault segments for large earthquakes $M_w \geq 5.9$ (Model-2).

Model-1: Historical Catalogs/Background Seismicity

In the background earthquake model spatially smoothed seismicity (Frankel, 1995; Frankel *et al.*, 1996) accounts for random earthquakes on unknown faults or on known faults for magnitudes below M_w 5.9. In its purest form, the smoothed-seismicity method simply assumes that patterns of historical earthquakes predict future activity, but it can easily be supplemented by tectonic or geodetically based zones or other model elements if there is reason to suspect that seismicity catalogs are insufficient.

We use the declustered historical catalogs prepared by the Working Group CPTI, (2004, Fig. 3) of $M_w \geq 4.6$ and higher, which consist of 2550 records of earthquakes in the time window from 217 B.C. to 2002 A.D. CPTI assigned a homogeneous magnitude to each earthquake from the three main types of magnitude available, M_s, M_w, and M_{sp} (Working Group CPTI, 2004). CPTI also identified periods of stationary completeness for different magnitude ranges.

The minimum magnitude of completeness, M_{min}, was chosen also as a minimum magnitude for the hazard calculations based on the common observation that in Italy the earthquakes with magnitude around 4.5 are likely to cause some damage; for example, Massa Martana (Umbria), 1997, M_d 4.5 (Frapiccini, 1997); Forlivese, 2000, M_L 4.3 (Camassi *et al.*, 2000); Valle dell'Aniene (Lazio), 2000, M_L 4.1 (Molin *et al.*, 2002). The M_{max} in this model was chosen as 5.9.

To obtain the maximum likelihood *a*- and *b*-value distribution (Weichert, 1980), the earthquakes were counted in several magnitude-time completeness. The *b* value determined was 0.90. Then the study area was divided into cells

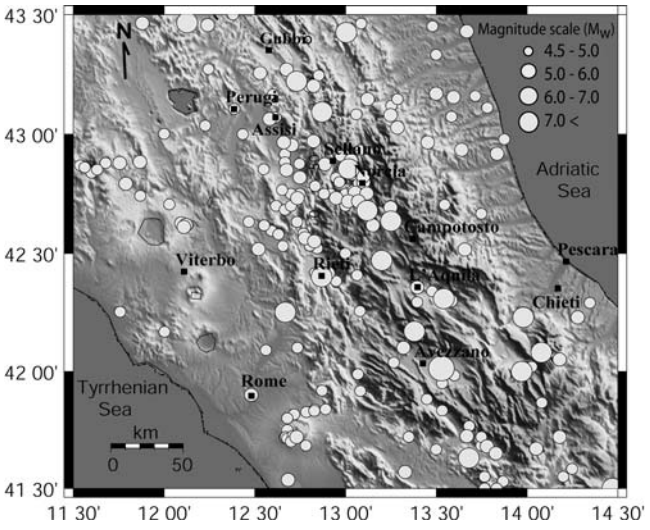

Figure 3. Location of earthquakes in the Working Group CPTI (2004) catalog from 271 B.C. to 2003 A.D., $M > 4.5$ together with the Apennine seismogenic master faults.

0.05° in latitude by 0.05° in longitude (roughly 5×5 km). We computed the gridded values (earthquakes/cell/year) and smoothed them spatially using a two-dimensional Gaussian function with a smoothing length of 25 km. This optimal distance was obtained by Console and Murru (2001) using a trial-and-error procedure. The seismicity fitted by the *a* and *b* values was allocated to the cells in proportion to the smoothed seismicity. This constitutes a 10^a grid.

Finally, using this grid, the annual rate of exceeding a specified ground motion at a site was calculated with the usual methods, using the computer codes available on the U.S. Geological Survey (USGS) Web site (see Data and Resources section). A maximum source-site distance of 150 km was chosen for the hazard calculations. (Because of the narrowness of Italy for cities in the study area, arcs of 150 km radius capture all the Apennine sources that are important in the ground-motion calculation.)

Model-2: Faults and Recurrence Models

Displacement of the Earth's crust along faults occurs either in the form of earthquakes or in aseismic creep (WGCEP, 2003). Because no evidence for aseismic creep is reported for the central Apennines, we ignore this possibility.

In PSHA models, the total seismic moment release for a fault source is sometimes partitioned between two different magnitude-frequency recurrence models, the characteristic (CH) or M_{max} model, which hypothesizes that the entire moment release is associated with a single M_{max}, and the Gutenberg–Richter model (GR), which considers earthquakes with a range of magnitudes between the minimum and M_{max} (Gutenberg and Richter, 1949). Together, these models are meant to incorporate our lack of knowledge about the specific fashion on which the earthquake activity takes place on a particular fault. In this study, however, we assume only the CH model for the faults and check whether this assumption is supported by the historical seismicity (see following section).

The Apennine faults are modeled in three dimensions using lengths, widths, depths, and dip angles. Table 1 gives the necessary information related with the 3D fault geometry (fault dip, *D*; depth, *H*; length, *L*; width, *W* and its seismic behavior, M_{max}).

For most of the Apennine faults, we assumed that the energy is released only by single segments that rupture independently, not together, in a cascade-type model. Figure 4 shows the fault segmentation model used in this study.

As well as the 1654 event mentioned earlier, many other historic earthquakes around M_w 5.9 cannot be assigned to specific faults (e.g., the 1654, 1747, 1751, 1799 events), and hence, they have been assigned to special, longer fault zones, for which the characteristic behavior is still assumed to be possible (faults 9, 16), but whose location is not known with sufficient precision. These earthquakes are assumed to rupture with a magnitude of M_w 5.9 anywhere along the fault with equal probability. These extended zones, termed float-

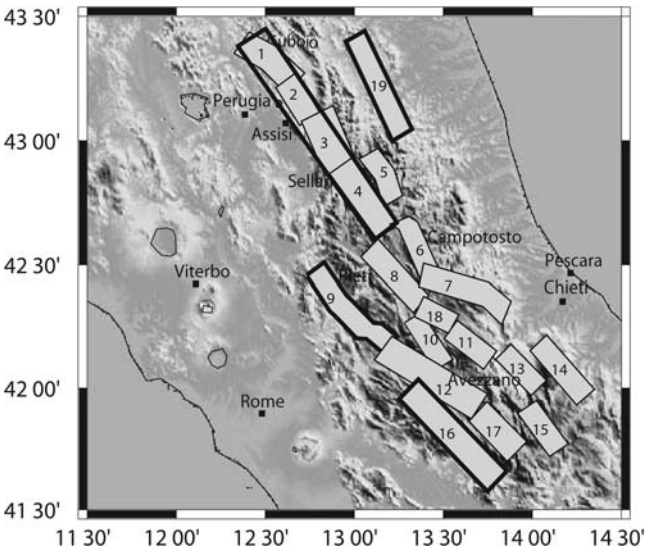

Figure 4. Fault segments used in this study for the central Apennines; boxes present the single characteristic earthquake segments (thin lines) as simplified rectangular shapes (detailed information on the scheme of a single box is given in Table 1. Thick lines present the fault zones in which we used the floating fault model. Fault segments are marked with numbers: **1**, Gubbio; **2**, Gualdo Tadino; **3**, Colfiarito, Sellano; **4**, Norcia; **5**, Mt. Vettore; **6**, Laga Mts. (Campotosto); **7**, Campo Imperatore Assegi; **8**, L'Aquila; **9**, Martani Mts. South, Salto-Velino Valleys; **10**, Ovindoli-Pezza; **11**, Middle Aterno Valley; **12**, Fucino; **13**, Mt. Morrone; **14**, Maiella; **15**, Aremogna–Cinquemiglia; **16**, Liri Valley–Sora; **17**, Upper Sangro Valley; **18**, Poggio Picenza; **19**, Fabrianese.

ing fault zones, are indicated in Figure 4 by thicker lines. The floating fault zones also account for uncertain geometry of the seismogenic source; for example, (1) The Fabriano–Camerino sector (number 19 in Fig. 4) where geologic data on the sources of the 1741 and 1799 earthquakes are lacking and (2) The Salto Valley–Rieti and Liri Valle–Sora sectors (numbers 9 and 16 in Fig. 4, respectively) where the segmentation is unknown, and geologic data seem to exclude the occurrence of large-magnitude events.

Note also that a floating fault zone is assumed in the area of sources 1, 2, 3, and 4 (Fig. 4) for some historical earthquakes whose historical location is not known sufficiently to be assigned to specific zones. This zone contains historical earthquakes with $M > 5.9$. Most of the M 5.9 earthquakes, for example, the ones that occurred in 1328, 1599, 1730, 1747, and 1859, cannot be accurately associated with faults by using geological and geophysical data. For these earthquakes that are not assigned to specific fault segments, we use a floating earthquake rupture model in order to calculate the seismic hazard, assuming that any of those eight earthquakes can rupture anywhere inside the long, specified zone with the same rate and probability (Fig. 4; Tables 1 and 2). The recurrence time for these earthquakes is calculated $RT = 103$ yr using a slip rate of 0.2 mm/yr. This means that one gets around 8–10 events in 800–1000 yr, assuming that the M_w 5.9 events are complete from around 1300. This number of events completely agrees with the number of earthquakes (eight) that occurred with M_w 5.9 in the zone (indicated by thicker lines in Fig. 4).

Nevertheless, inside the zone there are also four earthquakes with magnitudes greater than 5.9 that occurred in 500 A.D. (M_w 6.2, Gubbio), 1751 (M_w 6.3, Gualdo Tadino), 1279 (M_w 6.3, Colfiorito), and 1703 (M_w 6.8, Norcia) that can be associated with a fault segment identified by the geological and the geophysical data in the field. These four faults are modeled with the CH earthquake model assuming that each of them ruptures with its own calculated rate of occurrence and the characteristic magnitude at the same location (indicated by thinner lines in Fig. 4).

Thus, a total of five individual scenarios are inside the floating rupture zone. Four of them were computed using the CH model, and one of them is to be referred to the floating fault model introduced to the PSHA calculation separately with different rate of occurrence probability.

Comparison between Earthquake Rates Implied by Historic Earthquakes and the Geologic Source Model for the Central Apennines

Since a common test of a PSHA model is to compare the rate of earthquakes predicted from the source model to the historical record of earthquakes (Petersen *et al.*, 2000), we examine the difference between expected earthquake rates inferred from the historical earthquake catalog and the rates determined from the geologic data that were used to develop the seismic source model for the central Apennines including the rates associated with characteristic faults. In Figure 5 we show the total cumulative number of events per year greater than or equal to the magnitude predicted from the geologic source models (CH model for all sources), M_{pre}, together with the cumulative number of events per year ob-

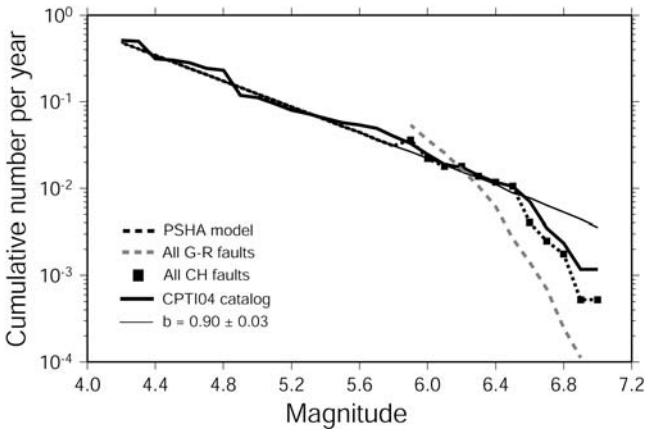

Figure 5. The cumulative number of events per year versus magnitude observed historically in the central Apennines (thick line) and predicted from our source model (dark dashed line). We also show the contribution to the predicted rates from the faults using the CH earthquake (square symbols) model and background seismicity sources (thin straight line).

served historically from the seismicity catalog, CPTI, and the final PSHA model for the central Apennines.

The Working Group CPTI (2004) catalog tends to follow a typical GR distribution, suggesting that the catalogs are complete for most of the range of magnitudes of interest. The thin straight line in Figure 5 indicates a GR model with a b value of 0.90. Note that our PSHA model rates and the historical seismicity rates are very similar for magnitudes below M_w 5.9 because one is derived from the other. Between magnitudes M_w 5.9 and M_w 6.5, faults treated as characteristic fit the historic curve better than faults treated as GR. For greater magnitudes, both the historic rate and the fault rates drop below the straight line given by the b value, the CH model giving the better fit.

Ground-Motion Prediction Equations

Ground-motion prediction equations (GMPEs) have been developed by Ambraseys *et al.* (1996) for the Mediterranean regions and by Sabetta and Pugliese (1996) for Italy through regressions of strong-motion data. Also, a set of empirical relationships is available for different geographical regions of Italy. These relationships were derived from the regional seismicity (weak- and strong-motion databases) containing thousands of waveforms recorded in areas with homogeneous attenuation characteristics (Malagnini and Herrman, 2000; Malagnini *et al.*, 2000, 2002; Bragato and Slejko, 2005; Morasca *et al.*, 2006). The new predictive ground-motion relationships recently developed by Malagnini *et al.* (2000) for the Apennines have been introduced into the hazard calculations together with the ones derived by Ambraseys *et al.* (1996) and Sabetta and Pugliese (1996).

We compare median predicted values from these GMPEs using some adjustments as described by Montaldo *et al.* (2005) because these equations use different definitions of different magnitude and distance scales. In particular, Montaldo *et al.* (2005) discuss the significance of the distance conversions and style-of-faulting adjustments as well as the problems related to the use of regional relations such as the selection of a reference depth, the quantification of random error, and the strong-motion prediction. In order to compare the PGA values for the same distance measurements, similar adjustments are obtained by Scherbaum *et al.* (2004). Simple approaches for adjusting predicted ground motions to compatibility in terms of magnitude, distance, etc., are presented by Bommer *et al.* (2005). Figure 6 shows the comparison between a PGA predicted by regional GMPEs (Malagnini *et al.*, 2000) for M_w 5.0 and M_w 7.0 with the results of the empirical regressions by Ambraseys *et al.* (1996) and Sabetta and Pugliese (1996). As can be seen in Figure 6, the Ambraseys *et al.* (1996) and Sabetta and Pugliese (1996) GMPE overestimate the PGA values compared to the regional GMPE one. The strong-motion based predictive relationships (Sabetta and Pugliese, 1996; Ambraseys *et al.*, 1996) are characterized only by a geometrical attenuation $1/r$ in the entire

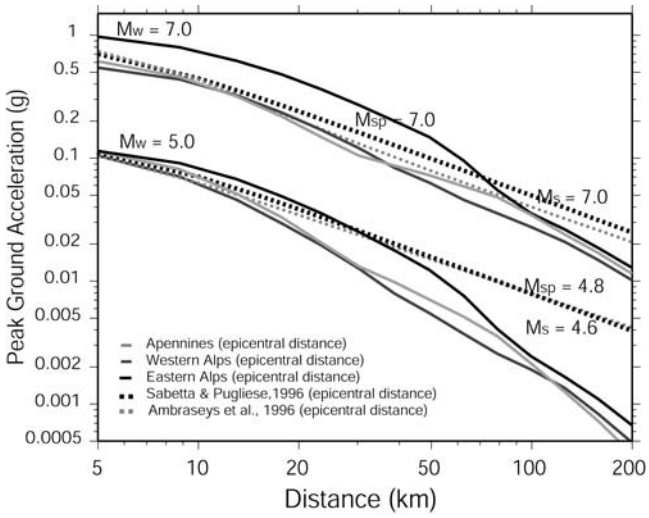

Figure 6. PGA computed for M_w 7.0 and M_w 5.0 earthquakes at a hard rock site. Results based on the attenuation and excitation parameters obtained by Malagnini *et al.* (2000, 2002) and Morasca *et al.* (2006, solid lines) are compared with the results of the empirical strong-motion regressions by Sabetta and Pugliese (1996, black dotted curves) and Ambraseys *et al.* (1996), gray dotted curves) after adjustments for compatibility.

distance range without anelastic attenuation. Such parameterization catches the average decay of the largest earthquakes, but it is unable to predict the motion amplitudes of smaller events for which the anelastic attenuation is more important. Because of the specific shape of the source radiation spectra, peak accelerations excited by large earthquakes are carried by low frequencies, whereas higher frequencies are responsible for carrying the peak accelerations of smaller events. The effect of the attenuation is thus much stronger on peak values of smaller events, and thus the discrepancy is observed for $M \leq 5.0$ events at larger distances.

These three GMPEs (Ambraseys *et al.*, 1996; Sabetta and Pugliese, 1996; Malagnini *et al.*, 2000) are incorporated into the calculations using a logic tree model and weighted. For the smoothed seismicity, we use only the regionalized GMPEs of Malagnini *et al.* (2000) with weight of 1.0 and for the faults, both (Ambraseys *et al.*, 1996; Sabetta and Pugliese, 1996) with weights of 0.5 each.

Occurrence Probability Models

The Time-Independent (Poisson) Model

The Poisson model is standard practice for most probabilistic seismic-hazard analyses, having been used most recently in the National Earthquake Hazard Maps for Italy (Stucchi *et al.*, 2004) as well as for the United States (Frankel *et al.*, 2002; Petersen *et al.*, 2008). In the Poisson model, the probability of occurrence of the next earthquake is independent of the time of occurrence of the previous one. The Poisson distribution has the important property of the hazard function that shows the conditional probability of an event

occurring, given that some interval has elapsed since the last even, is constant. Thus, it has no memory of the time of the most recent event. This assumption is reasonable when the hazard may depend on a number of different and independent sources. For sites near dominating faults, this assumption is questionable: an earthquake is not just as likely to occur on a fault segment one day after the most recent event as it is to occur on a day 200 yr later.

Time-Dependent (Renewal) Model

In contrast to the Poisson model, a time-dependent renewal process model is based on the assumption that after one earthquake on a fault segment, another earthquake on that segment is unlikely until sufficient time has elapsed to build sufficient stress for another rupture (Lindh, 1983; Sykes and Nishenko, 1984; Nishenko and Buland, 1987; Ellsworth, 1995; Ogata, 1999). Various statistical models have been proposed for the computation of the probability density function for earthquake recurrence, such as Gaussian, log-normal, Weibull, Gamma, and Brownian. In this study we use the BPT probability model that is based on a simple physical model of the earthquake cycle. In the BPT model, the failure condition of the fault is described by a state variable that rises from a ground state to the failure state during the earthquake cycle (Kagan and Knopoff, 1987; Ellsworth *et al.*, 1999; Matthews *et al.*, 2002). This model yields values that are very similar to the other time-dependent models except at elapsed times greater than the average recurrence interval.

The BPT model requires a minimum of two parameters as well as knowledge of the time of the most recent rupture. One parameter is the mean-recurrence interval, μ, and the other describes the variability of recurrence intervals and can be related to the variance of the distribution. This variability of recurrence intervals is described as the aperiodicity, α, which is related to the mean divided by the standard deviation.

The probability density for the BPT model is given by

$$f_{\mathrm{BPT}}(t) = \sqrt{(\mu/2\pi\alpha^2 t^3)}\,\exp[-(t-\mu)^2/2\alpha^2\mu t],$$

where t is time. The behavior of a BPT model depends strongly on the value of α. For smaller values of α, $f_{\mathrm{BPT}}(t)$ is more periodic, is strongly peaked, and remains close to zero longer. For larger values, the time in which the earthquake is very unlikely, the delay or dead time, becomes shorter, and $f_{\mathrm{BPT}}(t)$ becomes increasingly Poissonlike. The hazard function increases with decreasing values of α and becomes Poissonlike with increasing values that approach 1.0.

For the renewal model, the conditional probabilities for each fault are calculated. These probabilities are said to be conditional because they change as function of the time elapsed since the last earthquake. The 50 yr conditional probabilities, thus calculated, are converted to effective Poissonian annual probabilities by the use of following expression: $R_{\mathrm{eff}} = -\ln(1 - P_{\mathrm{cond}})/T$.

Aperiodicity Parameter

In the present study, we calculated aperiodicity parameter, α, from four sequences of repeating earthquakes in the central Apennines using an approach given by Savage (1991). In order to do so, we have to have enough interevent times to calculate a robust estimate of α. Ellsworth *et al.* (1999) has shown that sequences of only two or three intervals between events will be of little use for estimation of α. By restricting the sequences to those that have at least three and four closed intervals (i.e., five events), we found only three sequences out of all available in the Apennines suitable for analysis. The α values are around 0.22 for the Fucino and the Irpinia faults and around 0.50 for the Ovindoli–Pezza fault. Although the Iprinia fault is not listed in Tables 1 and 2 and not shown in Figure 1, it locates just in the southern part of the studied area. Because it has similar faulting features to the Fucino fault and has more than five dated paleoseismologic events from data observed in trenching studies (Pantosti *et al.*, 1993), we also used the Irpinia earthquake sequence to determine the aperodicity parameter.

Of course, these values are very uncertain, having been calculated from small samples, but their values serve to show the comparison with values found elsewhere. Ellsworth *et al.* (1999) found from statistical tests that (1) The limited worldwide earthquake recurrence interval data have a model shape factor (α value) of 0.46 ± 0.32, (2) The 35 recurrence interval sequences examined are compatible with a shape factor of 0.5, and (3) The 35 earthquake sequences had no systematic differences when grouped by tectonic style. Because we do not have experimental data of repeated earthquakes on the individual faults, and/or actual data on which to estimate aperiodicity in the central Apennines are sparse, we used the average value of α, 0.5, as a central value for the rest of the faults in the study region, and for a sensitivity study we also used this value with plus or minus 0.2, that is, 0.7, 0.5, and 0.3.

An illustration of how the α value affects time-dependent results is given in Figure 7 for the Aremogna–Cinquemiglia fault. For a time-dependent calculation, we present the time since the last earthquake as ratio of that time divided by the mean-recurrence interval of the earthquake (elapsed time ratio). For example, the current time is presented by time since the last earthquake over mean-recurrence time of the earth (1506 yr/1381 yr) = 1.09 for this fault. Generally, the conditional probability for α equal to 0.5 and 0.7 is closer to the fixed Poisson probability than the conditional probability for a α of 0.3. Also the conditional probability for a α equal to 0.7 and 0.5 rises above the Poisson probability level earlier in the recurrence cycle than the conditional probability for a α of 0.3. In general, the smaller the α, the nearer the rise in hazard above the Poisson level that the average recurrence time occurs.

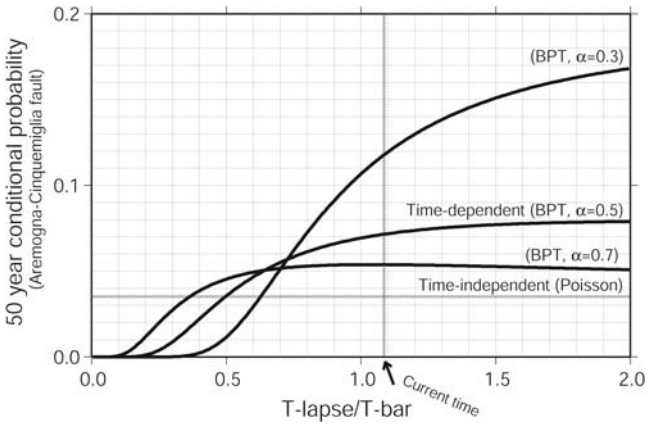

Figure 7. Graph showing 50 yr probability of the Aremogna–Cinquemiglia fault/earthquake occurrence as a function of elapsed time ratio. Curves are for Poisson model and BPT model with indicated α values. The x-axis presents lapse time since the last characteristic earthquake (T-lapse = 1506) as a ratio of the mean-recurrence interval (T-bar = 1381). The arrow indicates the 2006 lapse time for this segment.

In Table 2, we give the recurrence rates at each fault calculated using both the Poisson and BPT recurrence model. Seven of the 20 faults in Table 2 do not have the elapsed time, and the last earthquakes on these faults are assumed to have occurred in 500 A.D. (see Active Faults/Seismogenic Sources in the Central Apennines section). For these seven faults the elapsed times exceed the average calculated recurrence interval, and at the lowest α values, time-dependent probabilities are still sensitive to the elapsed time.

Hazard Computation

For earthquakes having magnitudes less than M_w 5.9, the source model is that of the smoothed seismicity. For earthquakes having magnitudes M_w 5.9 or greater, the source model is that of the characteristic faults. The computer codes used to make the hazard maps are taken from the Web site of the USGS (see the Data and Resources section). The methodology used follows that used by the USGS in the preparation of the U.S. national hazard maps. The codes used for the deaggregation calculation are taken from S. Harmsen (personal comm.) and modified for use in Italy.

Results

The Role of the Faults and the Background Seismicity

Figures 8a and b show, respectively, the hazard maps of mean PGA having 10% probability of exceedence in 50 yr on rock from Model-1 only, the background seismicity, and Model-2 only, the individual fault models. The map obtained using both models is shown in Figure 9d. The background seismicity contributes significantly to the hazard in the center of the study area and in some cases even dominates the

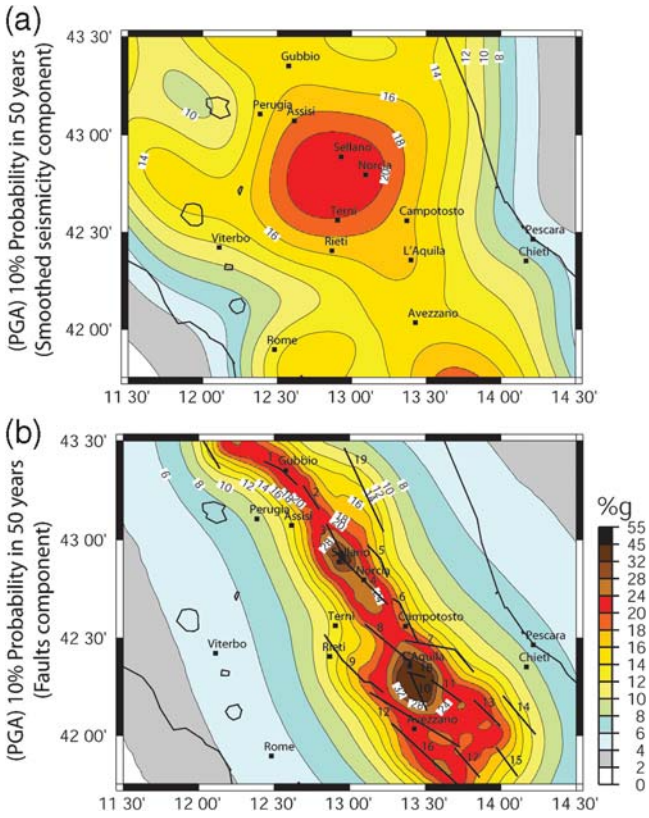

Figure 8. Maps of probabilistic PGA having 10% probability of exceedance in 50 yr for Poisson model derived from (a) gridded seismicity and (b) faults only.

contribution of the sources as we shall demonstrate in the deaggregations.

The Effect of Aperiodicity Parameter on the Hazard Maps

The results obtained for 10% probabilities of exceedence in 50 yr for PGA for the BPT ($\alpha = 0.3$, 0.5, and 0.7) and Poisson models are presented in Figure 9a–d. The differences between Poisson and BPT hazard are striking. In the Poisson model the hazard is not sensitive to the recency of rupture on the faults. Generally, but not always, time dependence raises the probabilities except for those faults that have had earthquakes recently (e.g., the Fuciuno, 1915). For example, the maps for PGA show high probabilistic accelerations in the Sellano and Norcia areas, around 0.32 g for the Poisson model, while the ground motions are lower, around 0.28 g for BPT model ($\alpha = 0.5$) since the elapsed time from the last earthquake for floating fault 1 was short (7 yr after 1997; see Table 2 and Fig. 9b). On the other hand, some source faults for high BPT conditional probabilities produce the most hazardous sites (for example, numbers 11, 13, 15, and 17 of Table 2 and Fig. 4). For example PGA is ~0.32 g around the city of L'Aquila for the time-independent model, while it increases nearly 60%–80%, up to 0.55 g, in the same

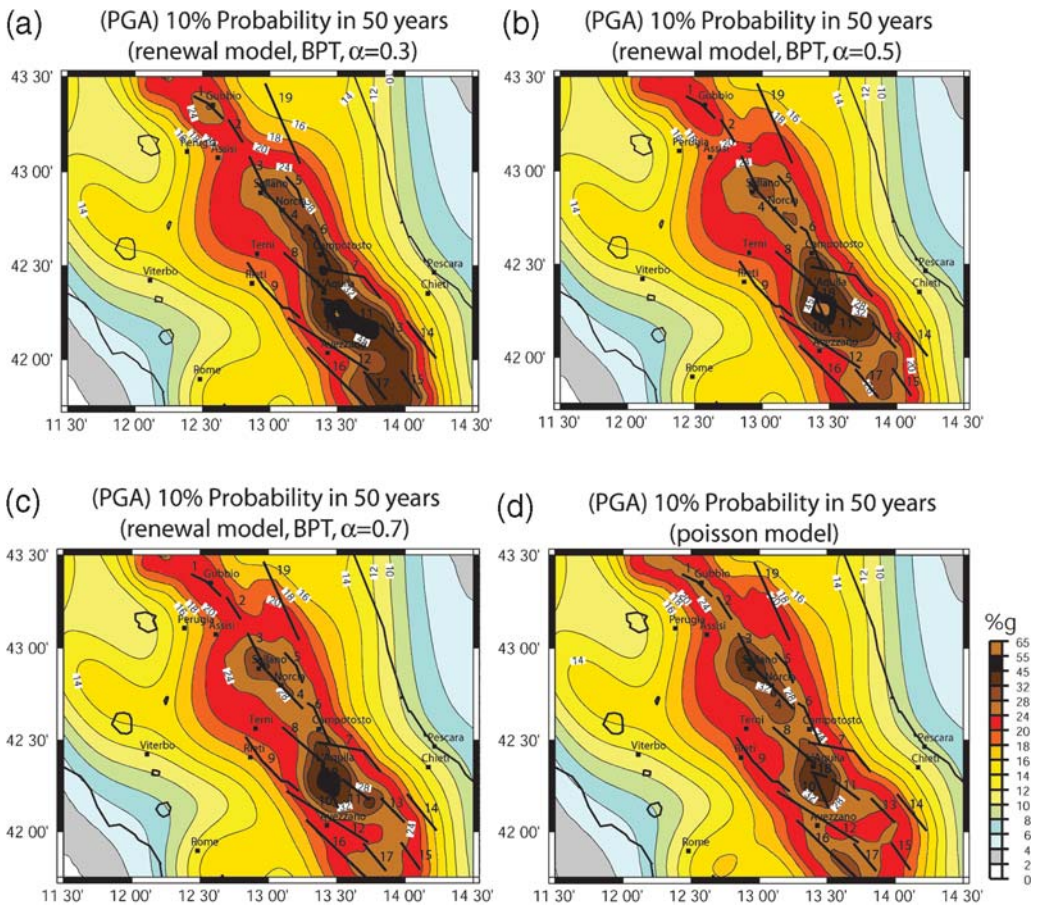

Figure 9. Maps of probabilistic PGA having 10% probability of exceedence in 50 years, derived from both gridded seismicity and faults BPT renewal model using the (a) $\alpha = 0.3$, (b) 0.5, (c) 0.7, and for (d) Poisson model.

site close to fault 11 for the time-dependent case ($\alpha = 0.3$) and becomes the most hazardous city in the study area.

From Figure 6 and Table 2, it is possible to estimate the effect of α on the hazard. In general, if the elapsed time is only a small fraction of the average recurrence time, the contribution of the fault to the hazard map will be small. Also, if the elapsed time is near or greater than the average recurrence time, the contribution of the fault to the hazard will increase with decreasing α. At values of elapsed time near 60% of the average recurrence time, the probability of earthquake occurrence can first increase and then decrease with decreasing α. When the steady contribution of the background seismicity is added into the model, great complexity is possible for the effect of decreasing α on the map values.

Just looking at sites near the center of each fault in Figure 9a–d, we have seen all of the following behaviors with decreasing α and suggest their likely causes in the following list.

1. Hazard increases continuously: one fault having elapsed time greater than the average recurrence interval dominates at the site.
2. Hazard decreases and then levels off: the domination of a fault having elapsed time shorter than average recurrence interval decreases to the point where the background seismicity dominates.
3. Hazard maintains a steady level: background seismicity always dominates.
4. Hazard stays level and then increases: background seismicity loses domination to a fault with elapsed time longer than the average recurrence interval.
5. Hazard stays level and then decreases: a fault having elapsed time shorter than average recurrence interval.
6. Hazard decreases and then increases: initially a fault having recurrence time shorter than the average recurrence interval dominates but then loses domination to another fault having elapsed time longer than average recurrence interval.
7. Hazard increases and then decreases: a dominating fault has elapsed time near 0.6 times the average recurrence time, a value where the probability of occurrence increases and then decreases as α goes from 0.7 to 0.5 to 0.3.

Overall, the PSHA results that are based on the time-dependent model display the effects of the recency of fault rupture by drastically reduced hazard levels in the northern sector and by somewhat elevated hazard levels in the southern sector.

Figure 10a–f shows the ratios (time-dependent over Poisson) for PGA and SA_1 hazard level of 10% exceedance in 50 yr where differences exceed 0.05 g using three separate α parameters 0.3, 0.5, and 0.7. Notice that α parameter has large influence on the results in each figure.

PGA estimates mostly increase with decreasing α at the southeastern part of the studied area including faults 7, 10, 11, 13, 15, 17, and 18, which have long lapse time that is well past average recurrence time (elapsed time ratio ~1.0). It decreases along the central belt of the Apennines where the faults have shorter lapse time of compared to its average recurrence time (fault 2, 4, 9, 12, and 16, elapsed time ratio ~0.0–0.2). In general, the choice of the α parameter creates small areas where the change is greater than 10% when $\alpha = 0.5$ and 0.7, and large areas where change is greater than 10% when $\alpha = 0.3$ (Fig. 10a–f). An α of 0.5 and 0.7 show changes less than 20%–25% in Figure 10b,c and 10e,f. Changes in the time-dependent maps both for PGA and SA_1 reach up to 60%–80% compared to time independent for $\alpha = 0.3$ depending on the recency of the last event on the fault that dominates at some sites (Figures 10a and d). From those figures, it is difficult to follow the details of the behavior of each fault as a function of elapsed time that may be observed in the deaggreation analysis (see following section).

Deaggregations

The process of deaggregation is that of the separation of magnitude and distance combinations that contribute to the exceedances of the map ground motion at a particular site. Deaggregation allows us to understand the magnitudes and distances that contribute the most to the hazard at a specific site and may help to select the design earthquake for such site. This information is often useful for engineering and planning purposes (McGuire, 1995).

Deaggregation for Rome and L'Aquila. We first deaggregated the seismic hazard for PGA and SA_1 at two sites in important urban areas, Rome and L'Aquila (Figs. 11a–d and 12a–d). In this study, we used the geographic deaggregation method that separates the contributions into bins of location, magnitude, and ground-motion uncertainty (Bazzurro and Cornell, 1999). We used equal area location bins with constant incremental radius and variable azimuthal angle (see Data and Resources section). In Figure 11a–d, 12a–d, and the following map views of deaggregated hazard, we show the geographic variation of hazard contribution both in terms of percent of the ground-motion exceedances (bar height) and average magnitude for the sources producing those exceedances in that bin (bar color).

For the city of L'Aquila, one or two magnitude location bins contribute over 50% of the ground-motion exceedances representing a single controlling source. Thus, the probabilistic hazard of L'Aquila is controlled by large earthquakes on faults located along the axis of the tectonic belt, and the L'Aquila fault contributes most to the PGA hazard.

For PGA with the Poisson model (Fig. 11a), faults 8 ($R \sim 0.1$ km), 10, and 18 ($R \sim 5$ km) contribute equally about 20%–30 % of the ground-motion exceedances. With the BPT model (Fig 11b) for $\alpha = 0.5$, the probabilistic ground motion at L'Aquila increases from 0.36 (Poisson) to 0.42*g* (time-dependent). The contribution from fault 8 decreases from 28% to 1% because the elapsed time is much smaller (elapsed time ratio = 0.22; see Table 2 and Fig. 7).

For SA_1 with the Poisson model and the BPT model, the behavior is essentially the same as for PGA.

In contrast to L'Aquila, for the city of Rome there is no single source that clearly dominates the seismic hazard. Both in the Poisson and BPT model for PGA, background seismicity contributes around 95% to the exceedance of the mapped ground motion (Figs. 12a and b).

For SA_1 the hazard contribution from distant faults 7, 10, and 12 ($R \sim 70$–90 km) becomes important, and the contribution from the background seismicity decreases almost 50% (Figs. 12c and d).

Paleoseismic evidence and seismic history suggest that the city of Rome has experienced considerable earthquake ground motion since its establishment more than 2000 yr ago. Seismic hazards in Rome are mainly associated with two active seismogenic areas, the Alban Hills and the central Apennines regions, located about 20 km southeast and 80–100 km east of central Rome, respectively. Within the past century, M_w 7.0 and M_w 5.3 earthquakes in the Apennines and the Alban Hills, respectively, generated intensities up to 7 in the city (Tertulliani and Riguzzi, 1995). This is reflected in the deaggregation results that show the PGAs to be dominated by moderate-sized background earthquakes ($M_w \sim 5.3$) at close distances (~20 km; Figs. 12a and b), whereas the 1.0 sec spectral accelerations predicted for Rome are also due to large earthquakes ($M_w \sim 6.8$–7.0) at distances of around 80–100 km, (Figs. 12c and d).

Deaggregation at Sites Illustrating Special Behaviors. Based on the hazard map behavior and knowledge of which faults ought to show increasing, decreasing, or more complex contribution to site hazard, and understanding that the background seismicity can disguise this behavior in the hazard maps, we selected three sites (A, B, and C) in which deaggregation shows the changing role of the fault and background sources as α gets smaller.

Site-A. For PGA with the Poisson model, the exceedance comes from fault 19 ($R = 10$ km), the closest fault, and from the background seismicity with contribution 59% and 36%, respectively (Fig. 13a).

In the BPT model, maximum ground motion decreases slightly from 0.17 to 0.15 g with decreasing α (Fig. 13b–d). The hazard contribution from fault 19 decreases with decreasing α and its elapsed time ratio is equal to 0.38. The

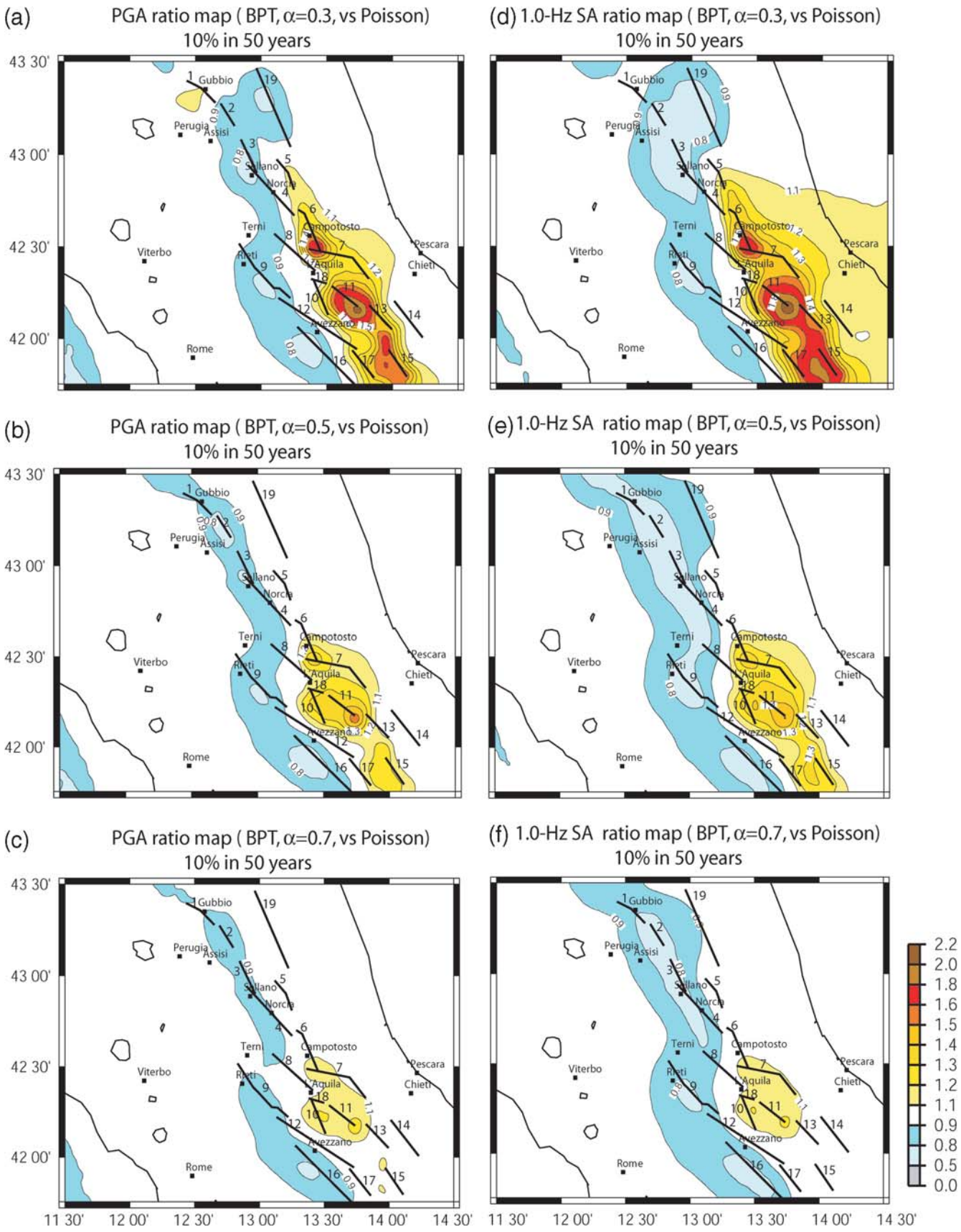

Figure 10. Maps of ratios of PGA (A, B, C, left) and SA_1 (D, E, F, right) hazard between time-dependent and Poisson models. Maps show ratios, BPT over Poisson model for 10% exceedance in 50-tear hazard, using different α values: (a, d) 0.3, (b, e) 0.5, and (c, f) 0.7.

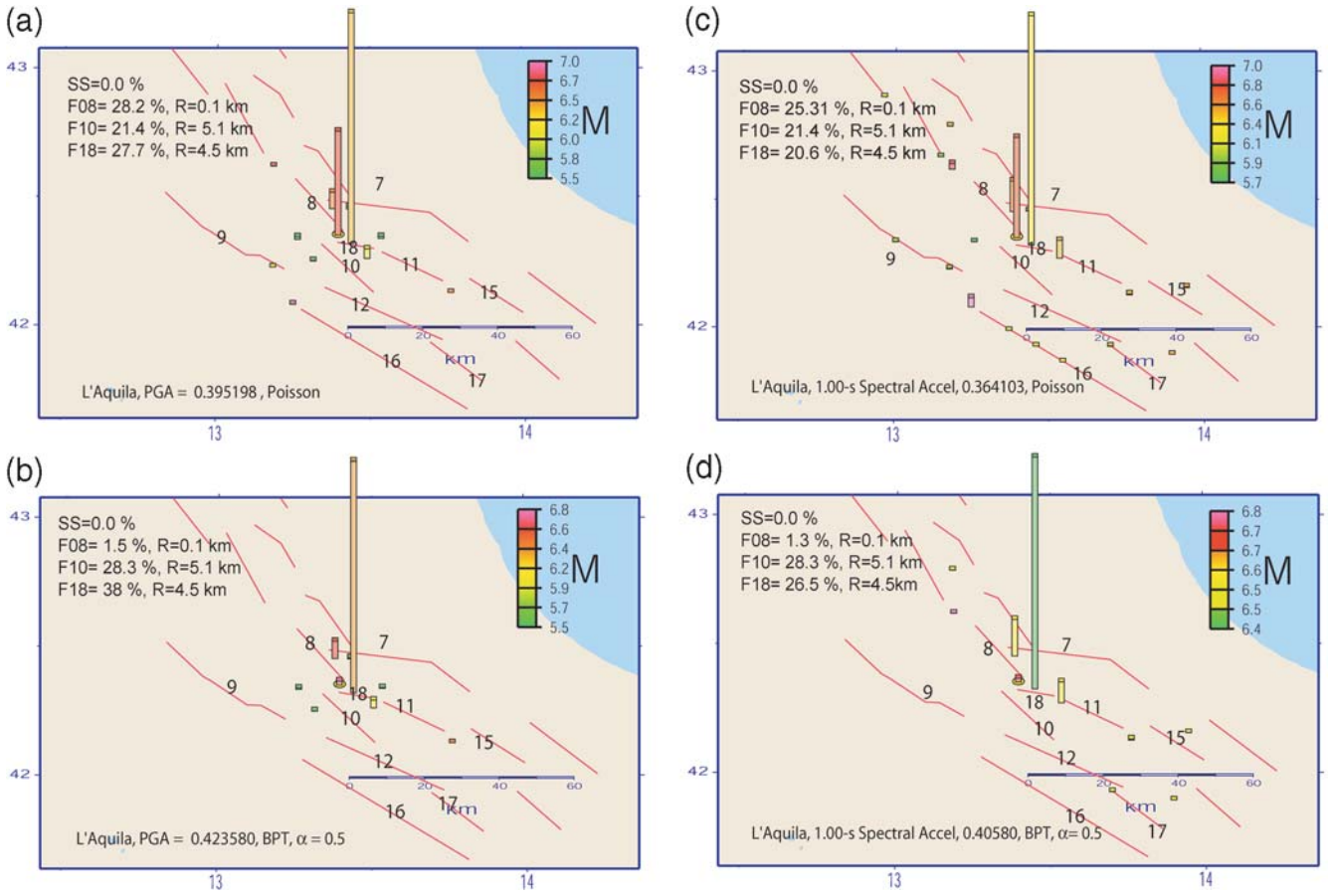

Figure 11. Deaggregated seismic hazard from BPT ($\alpha = 0.5$) and Poisson models for the city of L'Aquila (indicated with the yellow disk) for 10% in 50 yr probability of exceedance on crystalline rock with no site amplifications: PGA (a, b, left) and SA_1 (c, d, right). PGA and SA_1 are 0.39–0.42 g (PGA) and 0.36–0.41 g (SA_1) in L'Aquila, respectively. Here and figure 12, 13, 14, 15, 16, 17, and 18, the color of the bar over each location indicates the average magnitude of all potential seismic sources at that location. The height of the bar is proportional to the hazards from all sources at the location. Red lines represent surface traces of the faults. Major faults are numbered and correspond to one as given in Tables 1 and 2. ***F09***: Fault number 9, Fucino, as in Tables 1 and 2; Smoothed seismicity (***SS***).

contribution from fault 5 ($R = 32$ km) increases slightly when α decreases.

For this site for PGA, we see that the contribution of background seismicity is important both for the Poisson and the BPT cases. The BPT model slightly increases the hazard, and the dominating fault loses only a little domination.

For SA_1 with the Poisson model, the deaggregation is similar to that of PGA, but there is more contribution from distant faults 1, 2, 3, 5, 6, and 7 (Fig. 14a), a characteristic of deaggregations of longer-period ground motions. With the BPT model, the contribution from fault 19 decreases drastically from 40% to 12% with decreasing α. Behavior of faults 5 ($R = 32$ km), 6 ($R = 62$ km), and 7 ($R = 86$ km) is opposite. Their contribution increases to a maximum of 23%, 13%, and 7% with decreasing α, respectively because their elapsed times are well past the average recurrence times (Fig. 14b–d). This is a consequence of our assumption that when there is no known previous event, the date of the previous event is taken to be 500 A.D. giving a lapse time of more than 1500 yr.

For site SA_1 the background seismicity is important and becomes more so with the BPT model. The BPT model slightly decreases the hazard, and the dominating, closest fault loses its domination to more distant faults having larger lapse time.

Site-B. For PGA with the Poisson model (Fig. 15a), faults 11 ($R = 8.1$ km) and 10 ($R = 6$ km) contribute to the hazard at site-A equally with around 27% of the exceedences, and source 12 ($R = 12$ km) and the background contribute about 13% each.

For PGA with the BPT model, the hazard level increases from 0.26 to 0.34 g as α decreases (Fig. 15b–d). The contribution from fault 11 increases with decreasing α and reaches 66%, owing to the fact that its elapsed time since the last earthquake is well past the average recurrence time. The contribution of the other faults decreases either somewhat, as with fault 17, because of the moderate elapsed time, or completely as with fault 12 because it has had a recent event. The contribution of background seismicity, already minor, becomes much smaller.

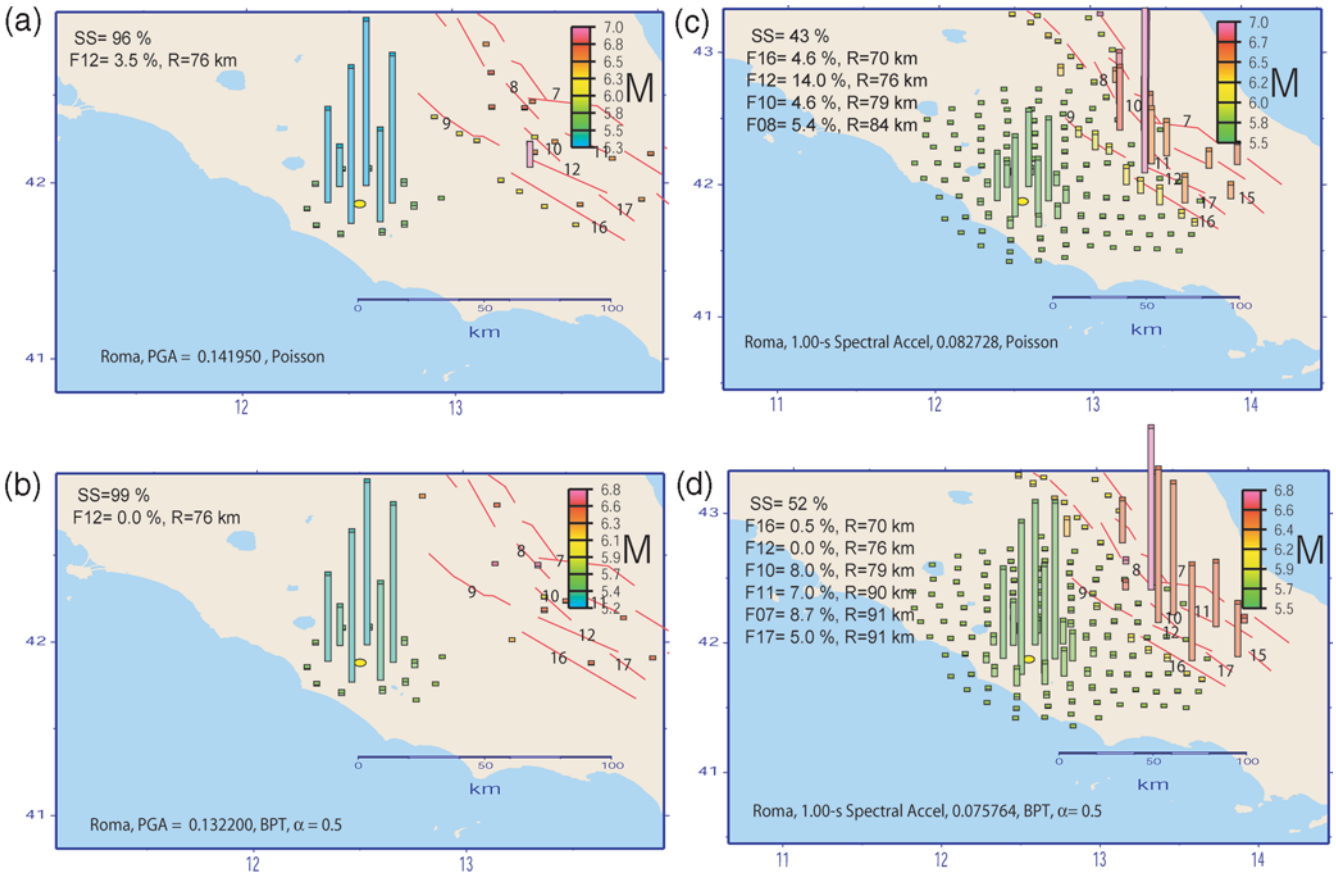

Figure 12. Deaggregated seismic hazard from BPT ($\alpha = 0.5$) and Poisson models for the city of Rome (indicated with the yellow disk) for 10% in 50 yr probability of exceedance on crystalline rock with no site amplifications: PGA (a, b, left) and SA_1 (c, d, right). PGA and SA_1 are 0.14–0.13 g and 0.080–0.075 g in Rome, respectively.

For SA_1 with the Poisson model, we observe contributions very similar to those of PGA but with slight contributions from more distant fault (Fig. 16a).

For SA_1 with the BPT model, the behavior is similar to that of PGA except that the domination of fault 11 is not as great, and the more distant ($R = 13.8$ km) fault 13 provides a greater contribution.

For this site, time dependence greatly increases the hazard. In contrast to site-A, for this site the background seismicity is not very important and becomes less important with decreasing α. The nearest fault (10) becomes less important, and a slightly farther fault (11) becomes dominating, while the role of more distant fault (12) becomes negligible.

Site-C. For PGA with the Poisson model, background seismicity contributes almost half the hazard, 44%, while faults at moderate distance contribute the rest (Fig. 17a). The primary fault contributions come from faults 7 and 14 at 36 km distance with 12%–15% of the exceedance. Other contributing faults are some that we saw contributing to site-B. The probabilistic ground-motion level is relatively low, which is why the more distant sources can equal the contribution of the local seismicity.

For PGA with the BPT model, the hazard increases only slightly (Fig. 17b–d). The contribution of the background seismicity decreases somewhat. Fault 14 loses all contribution as α gets smaller owing to an elapsed time only about half the average recurrence time. On the other hand, the percentage contribution of faults 7, 11, and 13 almost doubles because their elapsed times are well past their average recurrence time.

For SA_1 the primary effect when applying the Poisson model is that the background seismicity has only a minor contribution compared to the PGA case (Fig. 18a). The contribution of the mid-distant faults has increased because the longer-period ground motion is dominated by their larger magnitudes.

For the BPT model, the hazard at SA_1 increases about 15% (Fig. 18b–d). The minor contribution of the background seismicity stays constant while the role of the mid-distant fault is rather similar to the PGA case; fault 14 loses all contribution as α gets smaller while the percentage contribution of the other faults increases by 70% to 170%.

For this site, the role of the background seismicity depends on the ground-motion parameter—consistently important for PGA and consistently minor for SA_1 regardless of

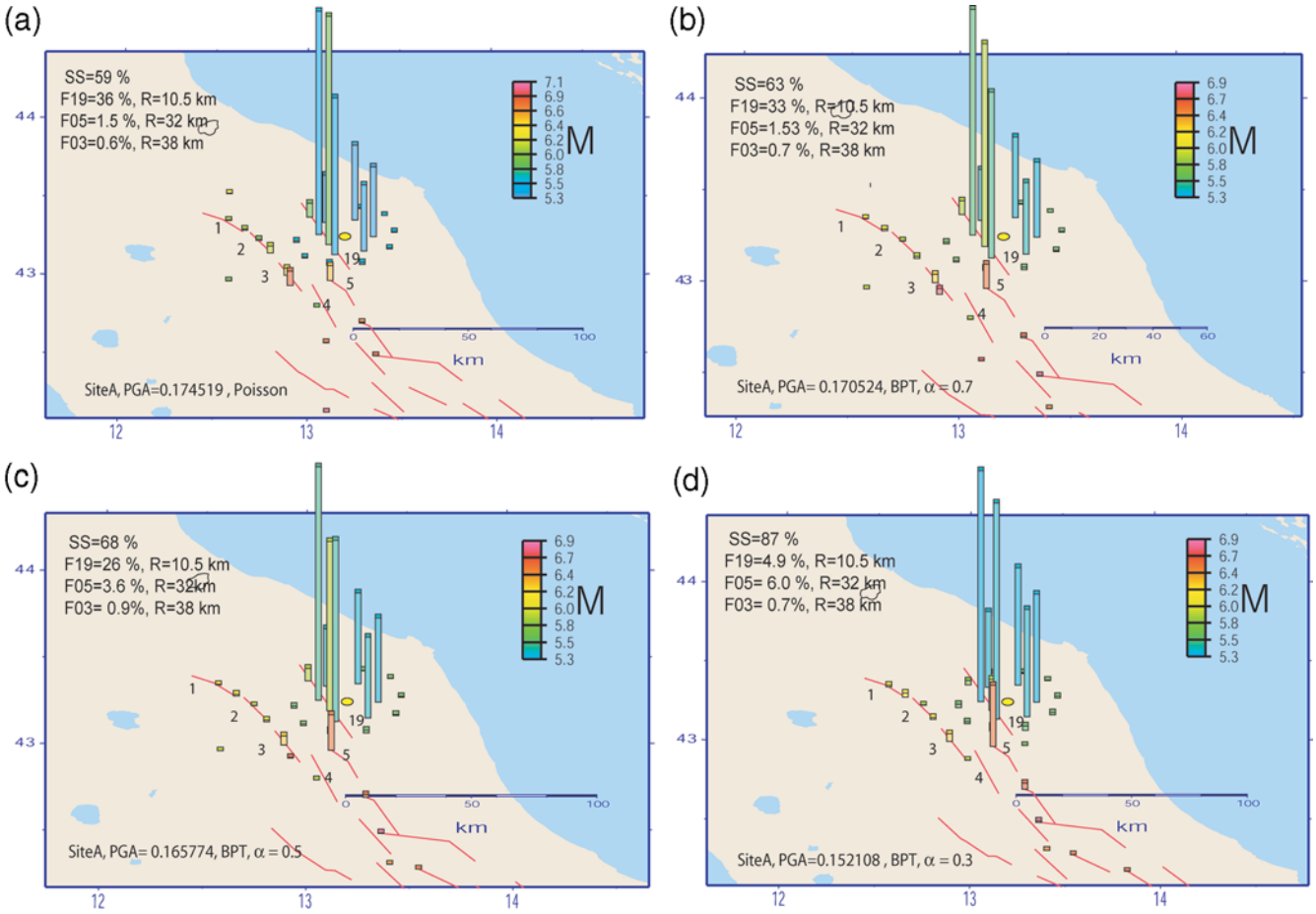

Figure 13 Deaggregated PGA hazard from (a) Poisson, and BPT for α, (b) 0.7, (c) 0.5, and (d) 0.3 models for ***site-A*** (indicated with the yellow disk) for 10% in 50 yr probability of exceedance on crystalline rock with no site amplifications.

recurrence model. The two closer of the mid-distance faults become either dominating or nil as α gets smaller, and the more distant faults increase their contribution.

General Behavior in Deaggregation. In deaggregation as a general behavior, we observe at each site: (1) Compared to PGA, SA_1 depends more on larger magnitudes and more distant sources, and (2) For either parameter, increasing the ground motions increases the dependence on closer sources. But when we examine the dominating sources at the sites considered, sources that might be candidates for deterministic design ground motions, we find a more complex and less predictable behavior.

For Rome and L'Aquila, it appears that the role of the background seismicity is dominant and nil, respectively, regardless of time dependence. For sites A, B, and C, we find that the role of the background seismicity can be large or small, can increase, can stay the same, or can even decrease with time depending on the ground-motion parameter. For all the sites, the dominating fault sources in the deaggregation shift under time-dependence depending on lapsed time/average recurrence time ratio. For this reason, the hazard may increase, stay the same, or decrease with time.

This complex behavior of hazard and dominating source suggests that when determining design ground motions, examination of the time-dependence is a necessary adjunct to deaggregation.

Discussion

Because probabilistic hazard maps will influence policy decisions on issues ranging from building codes to science funding, studies related to the uncertainty of map inputs and their effect on map values are important. Reliable probabilistic estimates demand that the uncertainties in alternative conceptual models be quantified (e.g., alternative approaches to constraining the relative rate of small and large-magnitude earthquakes). In this work, we have shown only the effect of uncertain earthquake occurrence models. Likewise, uncertainties in parameter values (e.g., ground-motion predictive models, fault geometries, maximum earthquake magnitudes, fault SR, or paleoseismic recurrence intervals) must be defined. By now, it is a common understanding among hazard practitioners that probabilistic seismic hazard is affected by large uncertainties that include not only those that are inher-

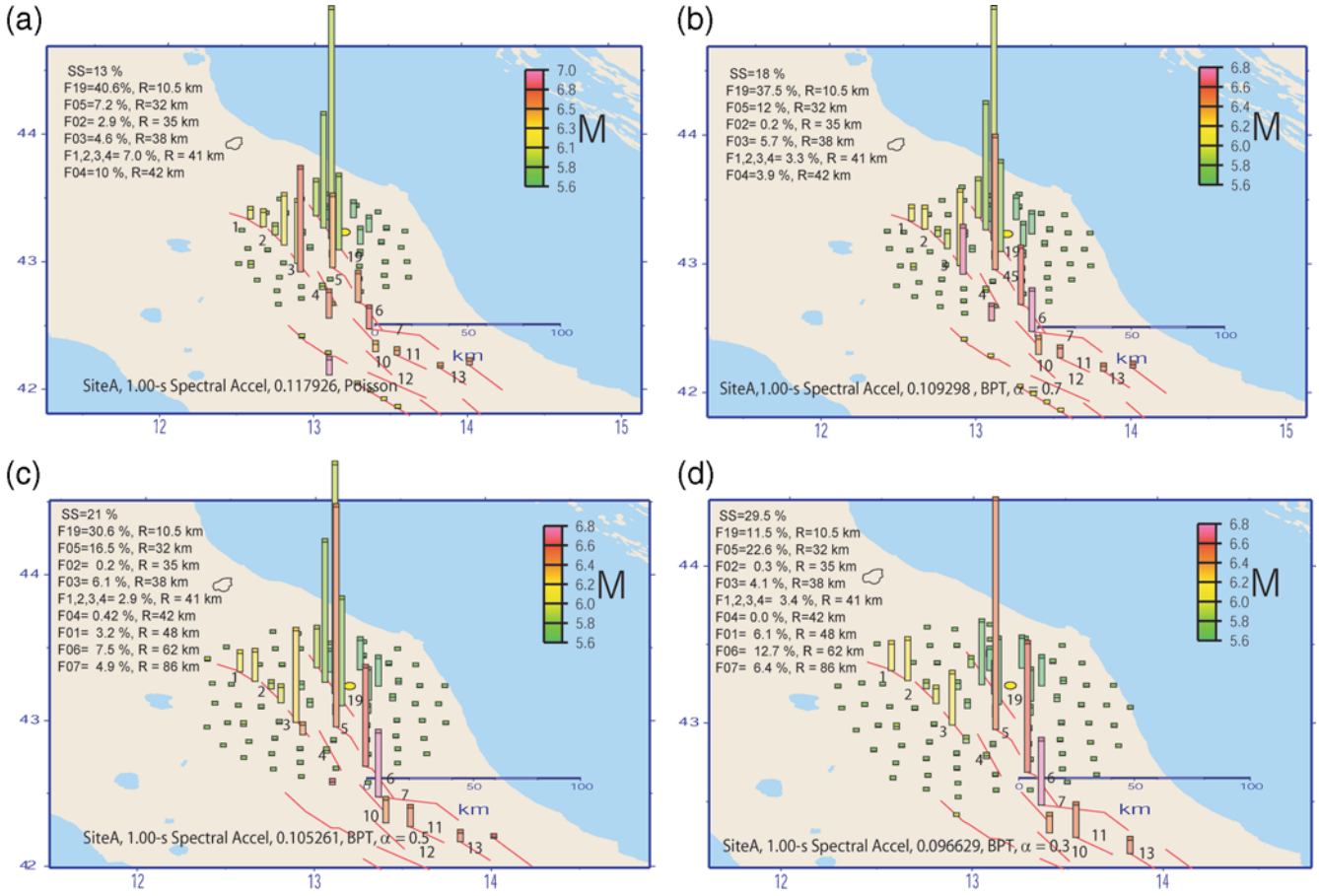

Figure 14. Deaggregated SA_1 hazard from (a) Poisson, BPT for α, (b) 0.7, (c) 0.5, and (d) 0.3 models for ***site-A*** (indicated with the yellow disk) for 10% in 50 yr probability of exceedance on crystalline rock with no site amplifications.

ent in the estimation of the input parameters but also those associated with the adopted source and model (Cramer *et al.*, 1996; Cramer, 2001; Beauval and Scotti, 2004; Bommer *et al.*, 2005; Cao *et al.*, 2005; Lombardi *et al.*, 2005; Morgan *et al.*, 2006; Akinci *et al.*, 2007, 2008). In order to provide a basis for assessing the uncertainty of the assessing priorities for critical research needed to increase reliability of future assessments, future effort will be devoted to defining and quantifying uncertainties in these parameters in a separate study.

We also compare our time-independent and time-dependent hazard maps with those generated by Pace *et al.* (2006) in the same area. First of all, we observe several areas with different hazard calculated following the smoothed-seismicity approach in two studies. Pace *et al.* (2006) calculate relatively high hazard with PGA around 0.2 g and 0.25 g in the areas, Lake Trasimeno (west of Perugia) and around the town of Chieti, where there is neither present nor historical seismic activity observed and calculated lower hazard around the Lake Bolsena, Viterbo (see their study; Figs. 2 and 10a) for which we observe the opposite feature in our study. This difference might be caused by the different *b* values but especially by the different GMPEs used in both studies. Pace *et al.* (2006) use spatially variable *b*-value distribution while we use the constant one. This high hazard observed in the Perugia and Chieti might be caused by unstable *b* values calculated from an insufficient number of earthquakes in their study. For the background seismicity based hazard, they use the Ambraseys *et al.* (1996) ground-motion relationship that overestimates the PGA values compared to the one predicted by the regional ground-motion relationship that is used in this study for smaller magnitudes (Akinci *et al.*, 2004; Lombardi *et al.*, 2005).

Differences between the time-independent hazard maps generated by the two studies might be caused by the use of different fault databases, fault parameters, and recurrence times. Moreover, differences between the two time-dependent hazard maps might be caused by the chosen elapsed time and α parameter. For example, we use different α values of 0.3, 0.5, and 0.7 in the time-dependent occurrence in order to explore its sensitivity to probabilistic ground motion, whereas Pace *et al.* (2006) calculate the α values from the statistics of alternative methods rather than from actual experienced recurrence times without using geological evidence at each individual fault. We do not believe that this procedure is correct.

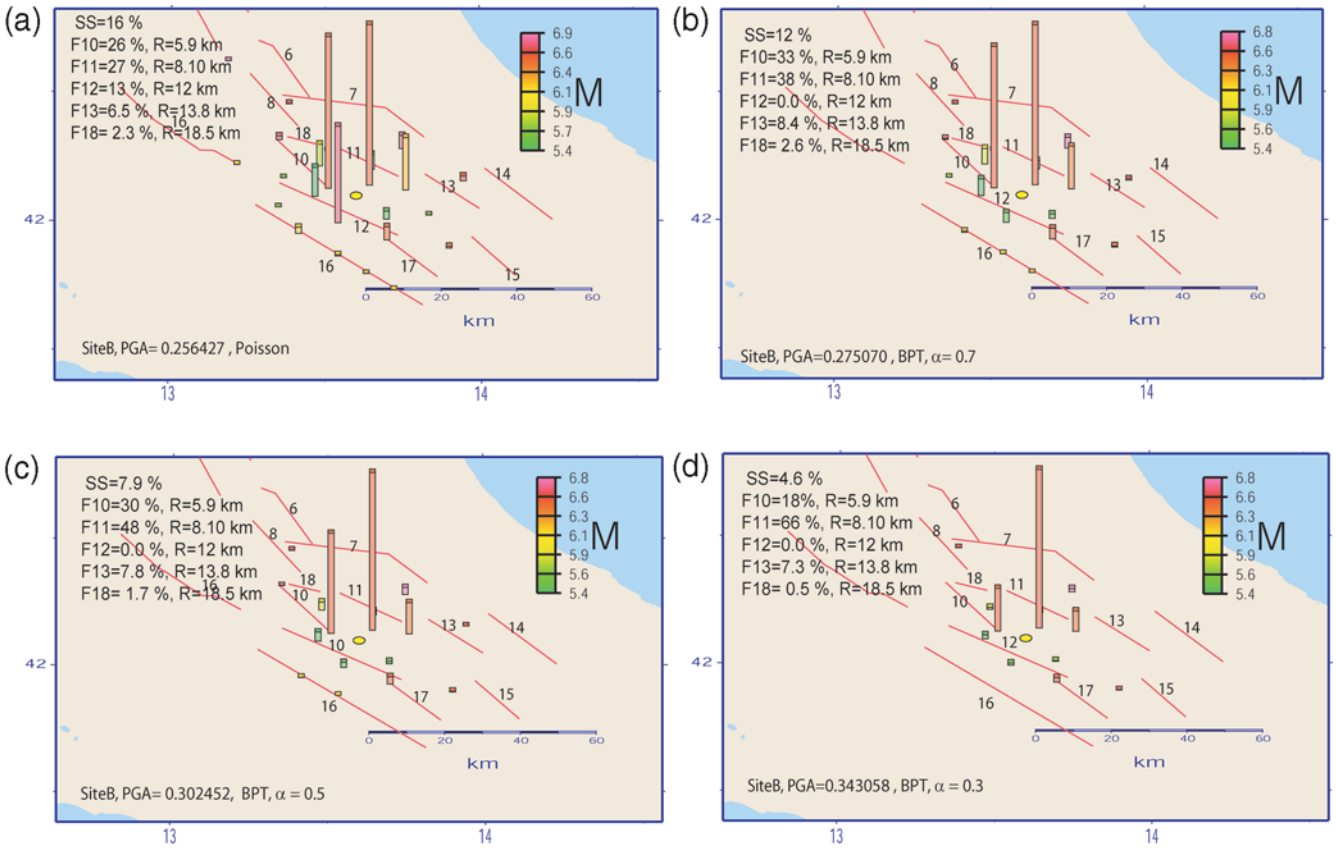

Figure 15. Deaggregated PGA hazard from (a) Poisson , and BPT for α, (b) 0.7, (c) 0.5, and (d) 0.3 models for ***site-B*** (indicated with the yellow disk) for 10% in 50 yr probability of exceedance on crystalline rock with no site amplifications.

Even though both studies use different geological and seismological databases and different α values, their general results are similar in the impact of the time-dependent model. That is, the contribution of the recently active source faults vanishes in the overall seismic hazard; the time-dependent PGA values are 20% lower than the Poissonian ones. On the contrary, some source faults with long elapsed time become the most hazardous sites, where the time-dependent PGA values are about 50% higher than those of the Poissonian model.

Because the two studies introduce different ingredients and parameters (GMPEs, seismicity catalogs, fault data base, earthquake occurrence models, α parameters, etc.) in the hazard calculations, it is difficult to identify the regions where the different estimates of hazard are caused by a specific parameter. We believe that this is an important issue to be studied in engineering seismology.

Influence of Geological Data Introduction

In this study, the hazard maps for the central Apennines are developed by combining geologic data that describe the long-term recurrence behavior of the major active faults with observation of the size and location of large historical earthquakes and seismicity data.

Overall, the match between the model seismicity and the historical seismicity is fairly good. The historical seismicity rates fall well within the rates calculated from geological data on the fault for the range of magnitudes, $5.9 \leq M_w \leq 6.7$, but the discrepancy becomes larger for magnitudes $M_w > 6.7$, and the fault source model underestimates the number of earthquakes above this magnitude level. This departure may indicate either that the larger earthquakes have recurrence intervals much longer than the historical records (hence, it is possible that three or four of them are missing for that reason) or that larger earthquakes are not possible for most Italian faults. The departure of our fault rates from the historical rate at the highest magnitude is not necessarily an underestimation of rate but could as well be the result of an event of long recurrence that happened to occur in the historical period or that the background accounts for a significant proportion of these events of $M_w > 6.7$.

Influence of the SR and the Recurrence Period

Considering the estimated SR used in this study we tried to answer the question, "Is there anything unusual about the faults having no major events in the past 1000 yr?" We looked at the median recurrence interval of the faults with one and no recurrence in the past 1000 yr, which is 1370 and 1429 yr, respectively. This is not significantly different.

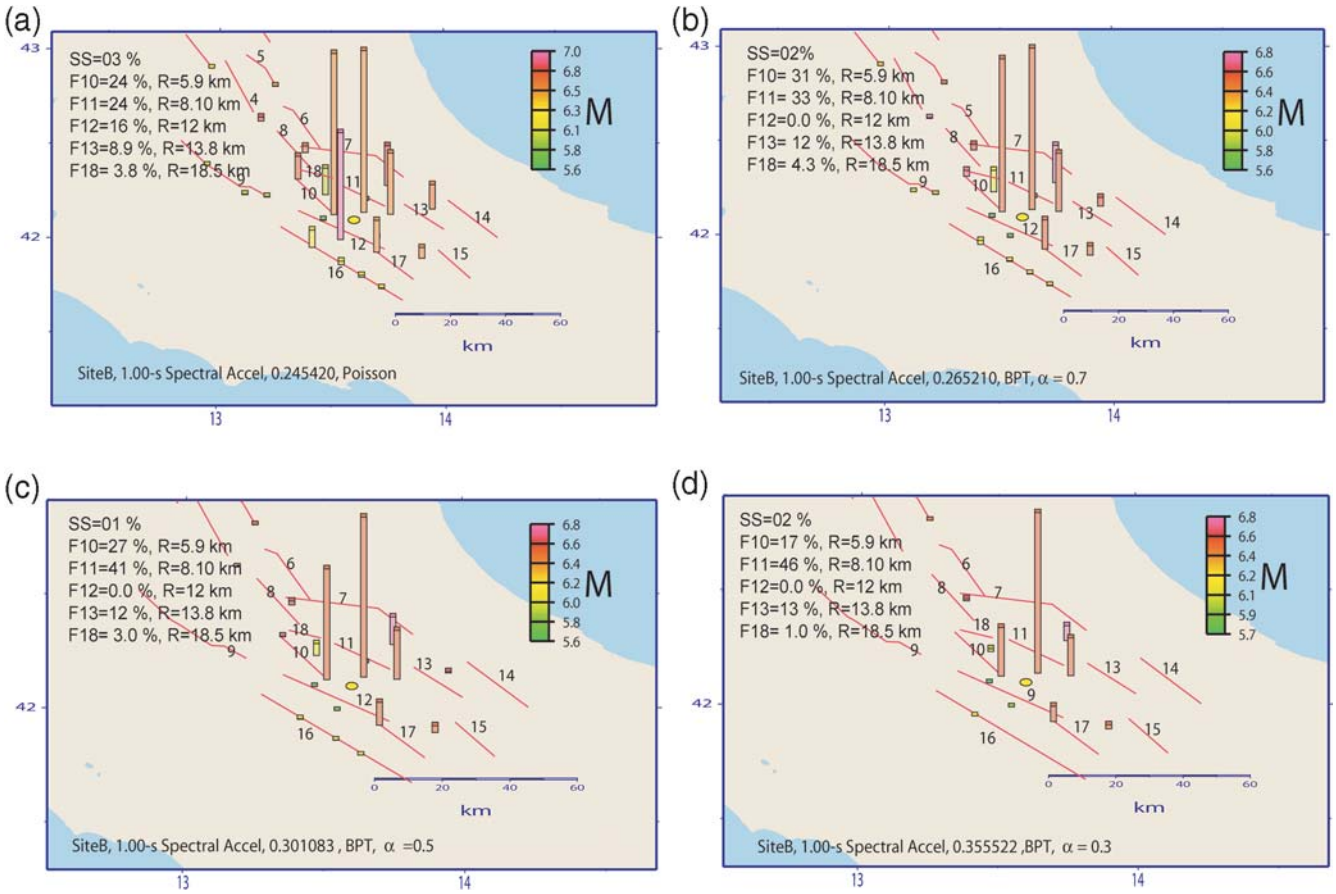

Figure 16. Deaggregated SA_1 hazard from (a) Poisson, BPT for α, (b) 0.7, (c) 0.5, and (d) 0.3 models for ***site-B*** (indicated with the yellow disk) for 10% in 50 yr probability of exceedance on crystalline rock with no site amplifications.

Assuming the estimated slip rate for each fault we calculated the probability of observing one or more events in 1000 yr for those faults in which one and no event were observed. The median value is 0.518 and 0.50 for those in which one or no event is observed in 1000 yr, respectively. These answers are consistent with the assumption that the assumed rates are consistent with observations. We simply expect about half of the faults to have experienced one or more events and half to have experienced no events in 1000 yr.

In this study, fault SR are converted to earthquake recurrence rates. The individual uncertainties on the slip rate that may cause variations in the recurrence parameters are not taken into account in the central Apennines. In our study, we have not assessed the uncertainty in hazard. Akinci *et al.*, (2008) show the effect of BPT and Poisson models together with uncertain SR and maximum magnitudes and hence recurrence times of the central Apennines. They observe that the uncertainty in occurrence probability under time-dependence is very large when measured by a ratio of the 84th to the 16th percentile, typically being as much as 2 orders of magnitude. On the other hand, when measured by standard deviation, these range from 2% to 6% for those faults whose elapsed time since previous event is large, but for faults with relatively recent previous occurrence, the probability of occurrence is always small, and hence, the standard deviations are less than 2%.

Influence of the Time Elapsed since the Last Event

Paleoseismological data and comparisons between the active fault framework and distributions of strong historical seismicity show that almost all faults (Fig. 1) in the western portion of the central Apennines were active during the past two millennia (Galadini and Galli, 2000). In contrast, data in the eastern portion of the investigated area indicate a lack of historical activity for most faults. The elapsed time since the last earthquake is, in such cases, longer than 1000 yr. For example; in the study region, for seven of the 20 faults we cannot assess an elapsed time, and the last earthquakes on these faults are assumed to have occurred in 500 A.D. with an elapse time of 1506. However, considering that the average recurrence interval for individual fault in the central Apennines is 1000–1500 yr (Table 2), a significant level of seismic hazard is related to these faults (Fig. 10a–f). Pace *et al.* (2006) imposed a 4000 yr elapsed time to those sources without a dated major event, taking into consideration the completeness stated by historical and archeological studies in central Italy but then treated those using Poisson as-

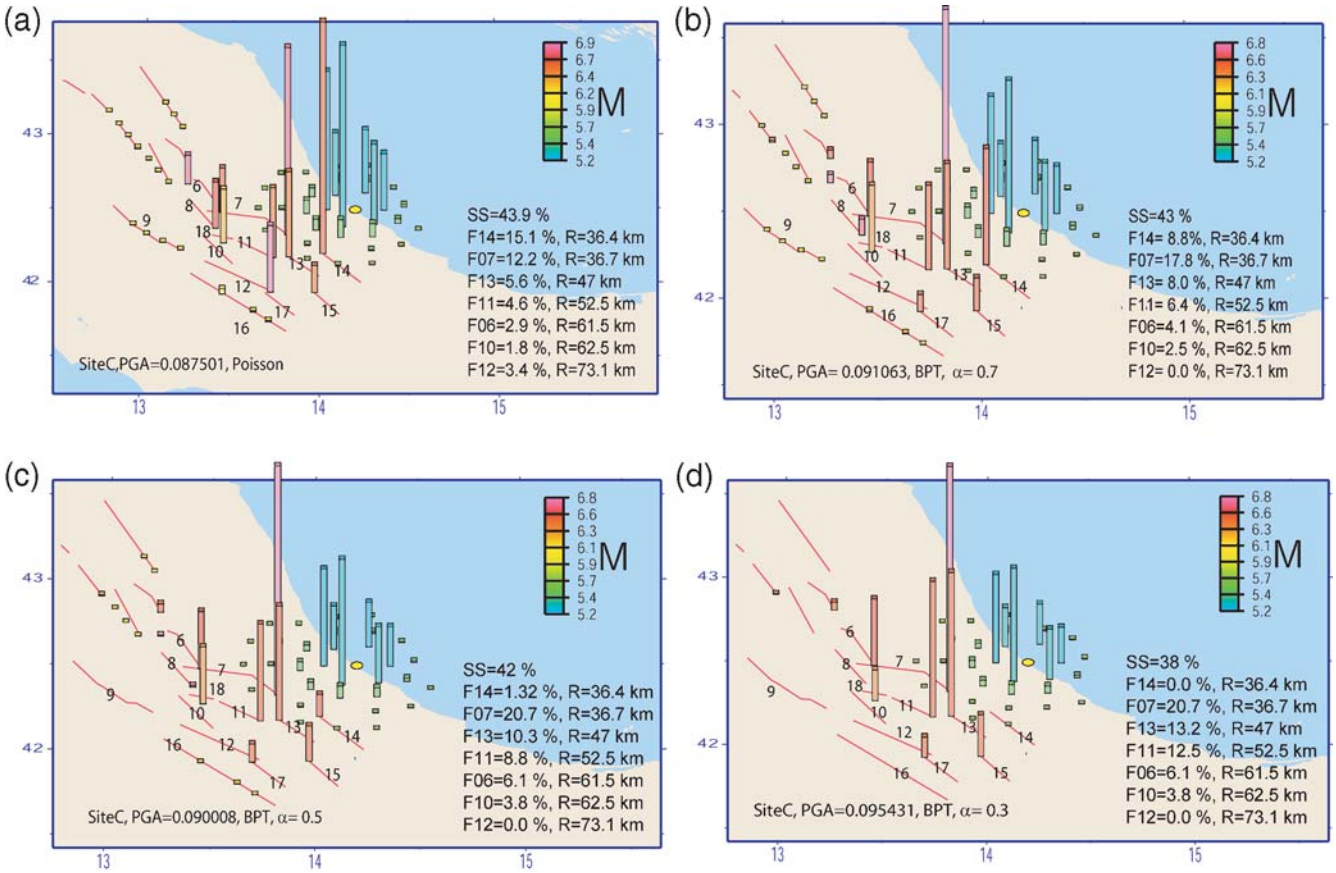

Figure 17. Deaggregated PGA hazard from (a) Poisson, BPT for α, (b) 0.7, (c) 0.5, and (d) 0.3 models for ***site-C*** (indicated with the yellow disk) for 10% in 50 yr probability of exceedence on crystalline rock with no site amplifications.

sumptions. Because the unresolved problems are already explained in this article, our parameters regarding magnitude and the faults associated with those magnitudes are different than used in the Pace *et al.* (2004) hazard calculations. Therefore, the differences between our models is that time-dependent hazard maps are mostly caused by the magnitude-frequency models (CH, GR, Poisson) used for calculating the hazard as well as by the parameters used for the problematic historical earthquakes/seismogenic sources in the region (referred to previous section on unresolved issues). Besides that, Pace *et al.* (2004) observed a similar behavior of sources that were recently active like Colfiorito and Fucino (activated during the 1997 and 1915, respectively) and diminished the overall hazard. On the other hand, some sources for the high BPT conditional probabilities become the most hazardous (in Pace *et al.* [2004] see faults called Campo Felice-Ovindoli, and Sulmona; in our study these faults correspond to Ovindoli and Mt. Morrone, respectively) and have longer lapse times compared to their return periods. Even though these two works cover the same area and assume similar behaviors of hazard, the PGA and SA can be quite different when one uses different aperiodicity parameter in the hazard calculations. In our study, we pointed out the impact of the different values of α and the deaggregation changes for the selected sites.

Influence of the Aperiodicity Parameter

In order to calculate the time-dependent hazard in the studied region, we have used the BPT model with three different aperiodicity parameters, 0.3, 0.5, and 0.7. These values are similar to the coefficient of variation of 0.5 ± 0.2 used by Working Group on Regional Earthquake Likelihood Model (RELM) of the Southern California Earthquake Center (SCEC, 1994). Sensitivity analysis on PGA and SA_1 shows impact of α parameters and time dependence versus time independence. The time-dependent maps for $\alpha = 0.7$ and 0.5 differ by about 10%–20% from the time-independent maps. The difference increases to $\pm 80\%$ when α gets smaller ($\sim$0.3, Fig. 10). However, for most of central Apennine located well away from the time-dependent sources, the ground motions are similar. The Mt. Morrone (number 13), Middle Aterno Valley (number 11), Upper Sangro Valley (number 17) and Aremogna–Cinquemiglia (number 15) faults that are located east-southeast of the central Apennines generally have elevated hazard relative to the time-independent maps. This is because it has been a long time

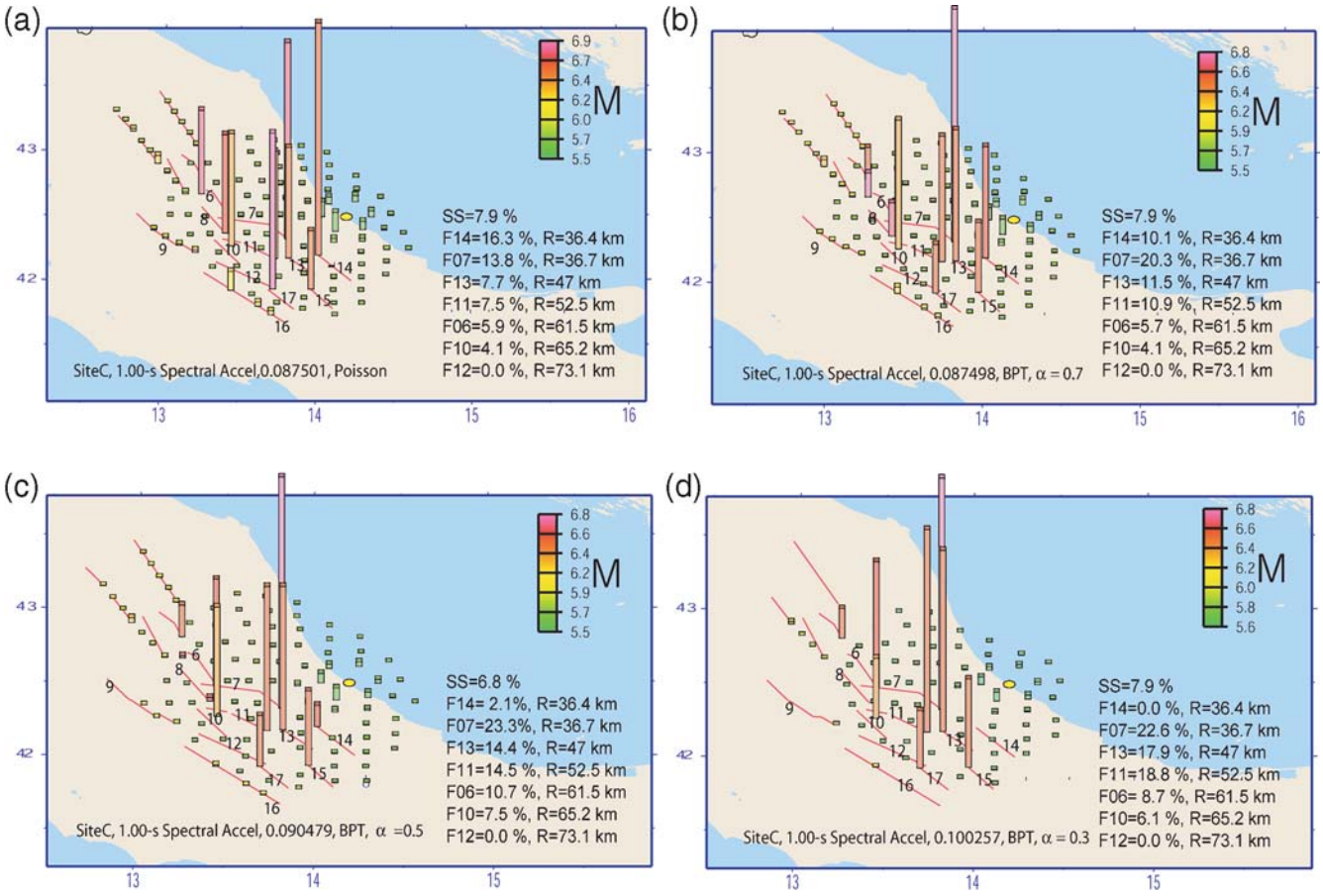

Figure 18. Deaggregated SA_1 hazard from (a) Poisson, BPT for α, (b) 0.7, (c) 0.5, and (d) 0.3 models for ***site-C*** (indicated with the yellow disk) for 10% in 50 yr probability of exceedence on crystalline rock with no site amplifications.

since the last earthquake, about 1500 yr since the 500 A.D. assumed activation. All of these faults are late or close to their seismic cycles. The Gualdo Tadino (number 2), Fucino (number 12), Norcia (number 4), Liri Valley–Sora (number 16) faults, on the other hand, have time-dependent hazard that is lower than the time-independent hazard due to the relatively short period since the last earthquake that places these faults in the first half of their seismic cycles.

Importance of Deaggregations

Seismic-hazard analyses for engineering purposes are usually conducted for particular sites rather than regions. Because of this, there has been a move to make hazard assessments as site specific and as fault specific as possible. Deaggregation plots can provide useful information on how the typical size and distance of earthquakes making the largest contributions to the seismic hazard at a specific site varies both with the probability level and with the spectral parameter. Performing deaggregations at more than one period will help determine if one source dominates at all periods and clarify the need for one or more design earthquakes. This information can also be used to generate the scenario earthquakes and the corresponding time histories for dynamic seismic design and retrofit for cities in the central Apennines, Italy (Olsen *et al.*, 2006). These maps may assist in the determination of earthquake parameters (magnitude and distance) that earthquake engineers use in their work in earthquake-resistant design and retrofitting. We also observed that larger, more distant earthquakes are more important contributors to the SA_1 hazard than the PGA hazard. This typical behavior is seen in the deaggregation for the cities of Rome, L'Aquila, and the selected three sites. This is caused by the higher ratio of long-period to short-period energy radiated by larger earthquakes and to be lower rate of amplitude decay per unit distance for long-period waves.

Conclusions

We constructed a PSHA model for the central Apennines based on the long-term recurrence behavior of active faults together with the spatial distribution of earthquakes observed in historic time. In order to express the time dependence of the seismic processes to predict the future ground motions in the region, we used a BPT model (Matthews *et al.*, 2002). We presented the results for both BPT and Poisson models in terms of maps of PGA and SA_1 for 10% probability of ex-

ceedance in 50 yr. The maps show the highest levels of PGA and SA to occur along the axis of the tectonic belt both for the time-dependent and the time-independent models. Time-dependent hazard is increased with respect to the results of the Poissonian source model, and the peaks appear to shift to the east-southeast of the central Apennines. Using aperiodicity parameter (α) of 0.3, 0.5, and 0.7, we examine the sensitivity of the probabilistic ground motion to these parameters. PGA estimates mostly increase with decreasing α at the southeastern part of the studied area including the faults 7, 10, 11, 13, 15, 17, and 18 that have long lapse times well past average recurrence time (elapsed time ratio ~1.0). The hazard decreases along the central belt of the Apennines where the faults have shorter lapse of time compared to its average recurrence time (faults 2, 4, 9, 12, and 16, elapsed time ratio ~0.0–0.2).

Because it is difficult to follow the details of the behavior of each fault as a function of elapsed time, we deaggregated the seismic hazard at some specific sites as a function of α parameter. When we examined the dominating sources at the sites considered, sources that might be candidates for deterministic design ground motions, we found quite complex and less predictable behavior. We observed at each site compared to PGA, SA_1 depends more on larger magnitudes and more distant sources, and for either parameter, increasing the ground motions increases the dependence on closer sources. This complex behavior of hazard and dominating source means when determining design ground motions, examination of the time dependence is a necessary adjunct to deaggregation.

The results of the present study clearly illustrate the influence of active fault parameters to probabilistic seismic-hazard maps. However, the absolute ground-motion levels obtained in this study should be considered with care since these are highly dependent of the assumptions made in the different input models and the chosen attenuation relation.

In general, the time-dependent models may be applicable in a few areas because we know little about the recurrence rates for the majority of seismic sources in most regions of the world. However, for the few faults for which we think we have adequate information on time-dependent behavior, a time-dependent model may be better than a time-independent model at identifying the short-term risks for economic loss assessment.

Data and Resources

In this article we used declustered CPTI (2004) historical catalog prepared by the Working Group (http://emidius.mi.ingv.it/CPTI04, last accessed May 2007). Fault information used for hazard calculations (Tables 1 and 2) came from many published sources listed in the references. The annual rate of exceeding a specified ground motion at a site was calculated using the computer codes available on the USGS Web site (http://earthquake.usgs.gov/research/hazmaps/, last accessed December 2008). Many of the plots are made using the Generic Mapping Tools version 4.2.1 (www.soest.hawaii.edu/gmt, last accessed December 2008; Wessel and Smith, 1998) We used equal area location bins available on the USGS Web site (http://eqint.cr.usgs.gov/deaggint/2002/index.php, last accessed May 2007, December 2006, and December 2006, respectively).

Acknowledgments

The thoughtful reviews by Arthur D. Frankel and Steve Harmsen of United States Geological Survey (USGS), Golden, Colorado, whom we wish to thank, strongly contributed to the clarity and the readability of this article. We would also thank Editor-in-Chief Andrew J. Michael, Mark W. Stirling, and an anonymous reviewer whose comments and suggestion improved the manuscript. During this work at the USGS in Golden, Colorado, A. Akinci and D. Perkins at Istituto Nazionale di Geofisica e Vulcanologia in Rome, Italy, were supported by grants from the Consiglio Nazionale delle Ricerce and Civil Protection Projects, (DPC-S2), 2004–2006.

References

Akinci, A., C. Mueller, L. Malagnini, and A. M. Lombardi (2004). A probabilistic seismic hazard assessment for the Alps and Apennines (Italy) using historical seismicity and new predictive ground-motion relationships, *Boll. Geofis. Teor. Appl.* **45,** no. 4, 285–304.

Akinci, A., D. Perkins, and A. M. Lombardi (2007). A Monte Carlo approach in estimating endogenous uncertainties for a seismic hazard assessment of the central Apennines, Italy, in *Seism. Res. Lett.*, *Seismological Society of America, Annual Meeting*, **78,** no. 2.

Akinci, A., D. Perkins, A. M. Lombardi, and R. Basili (2008). Uncertainties in the estimation of the probability of occurrence of strong earthquakes from individual seismological sources in the Apennines, Italy, *J. Seism.*, doi 10.1007/s10950-008-9142-y (in press).

Ambraseys, N. N., K. A. Simpson, and J. J. Bommer (1996). Prediction of horizontal response spectra in Europe, *Earth. Eng. Struct. Dyn.* **25,** 371–400.

Barchi, M., F. Galadini, G. Lavecchia, P. Messina, A. M. Michetti, L. Peruzza, A. Pizzi, E. Tondi, and E. Vittori (a cura di) (2000). Sintesi delle conoscenze sulle faglie attive in Italia centrale, *CNR—Gruppo Nazionale per la Difesa dai Terremoti*, 62 pp.

Basili, R., G. Valensise, P. Vannoli, P. Burrato, U. Fracassi, S. Mariano, M. M. Tiberti, and E. Boschi (2008). The database of individual seismogenic sources (DISS), version 3: summarizing 20 years of research on Italy's earthquake geology, *Tectonophysics* **453,** no. 1–4, 20–4.

Bazzurro, P., and C. Cornell (1999). Disaggregation of seismic hazard, *Bull. Seismol. Soc. Am.* **89,** 501–520.

Beauval, C., and O. Scotti (2004). Quantifying sensitivities of PSHA for France to earthquake catalog uncertainties, truncation of ground-motion variability, and magnitude limits, *Bull. Seismol. Soc. Am.* **94,** 1579–1594.

Bertini, T., and C. Bosi (1993). La tettonica quaternaria della conca di Fossa (L'Aquila), *Il Quaternario* **6,** 293–314.

Blumetti, A. M. (1995). Neotectonic investigations and evidence of paleoseismicity in the epicentral area of the January–February 1703, central Italy, earthquakes,, in L. Serva and D. B. Slemmons (Editors), *Perspectives in Paleoseismology*, Association of English Geologists, Spec. Publ., no. 6, 83–100.

Bommer, J. J., F. Scherbaum, H. Bungum, F. Cotton, F. Sabetta, and N. A. Abrahamson (2005). On the use of logic trees for ground-motion prediction equations in seismic-hazard analysis, *Bull. Seismol. Soc. Am.* **95,** 377–389.

Boncio, P., G. Lavecchia, and B. Pace (2004). Defining a model of 3D seismogenic sources for seismic hazard assessment applications: the case of central Apennines (Italy), *J. Seism.* **8,** 407–425.

Boncio, P., G. Lavecchia, G. Milana, and B. Rozzi (2004). Seismogenesis in central Apennines, Italy: an integrated analysis of minor earthquake sequences and structural data in the Amatrice-Campotosto area, *Ann. Geophys.* **47,** 1723–1742.

Bosi, C. (1975). Osservazioni preliminari su faglie probabilmente attive nell'Appennino centrale, *Boll. Soc. Geol. It.* **94,** 827–859.

Bosi, C., and T. Bertini (1970). Geologia della media valle dell'Aterno, *Mem. Soc. Geol. It.* **9,** 719–777.

Bragato, L., and D. Slejko (2005). Empirical ground-motion attenuation relations for the eastern Alps in the magnitude range 2.5–6.3, *Bull. Seismol. Soc. Am.* **95,** no. 1, 252–276.

Camassi, R., and V. Castelli (2004). Looking for "new" earthquake data in the 17th–18th century European "newssellers" network, *J. Earthq. Eng.* **8,** 335–359.

Camassi, R., P. Galli, D. Molin, and A. Tertulliani (2000). Eventi sismici del faentino forlivese dell'aprile-maggio 2000 e del Reggiano del 18 giugno 2000, Rilievo macrosismico, *Rapporto interno ING-SSN, Roma*, 16 pp.

Cao, T., M. Petersen, and A. Frankel (2005). Model uncertainties of the 2002 update of California seismic hazard maps, *Bull. Seismol. Soc. Am.* **95,** 2040–2057.

Carraro, F., and M. Giardino (1992). Geological evidence of recent fault evolution. Examples from Campo Imperatore (L'Aquila-central Apennines), *Il Quaternario* **5,** 181–200.

Carrara, C., G. DaiPra, and C. Giraudi (1995). Lineamenti di tettonica plio-quaternaria dell'area, in *Lazio Meridionale, Sintesi delle Ricerche Geologiche Multidisciplinari*, Dipartimento Ambiente, ENEA, Rome, 151–155.

Cavinato, G. P., and E. Miccadei (1995). Sintesi preliminare delle caratteristiche tettoniche e sedimentarie dei depositi quaternary della conca di Sulmona (L'Aquila), *Il Quaternario* **8,** 129–140.

Chiaraluce, L., M. Barchi, C. Collettini, F. Mirabella, and S. Pucci (2005). Connecting seismically active normal faults with quaternary geological structures in a complex extensional environment: the Colfiorito 1997 case history (northern Apennines, Italy), *Tectonics* **24,** TC1002, doi 10.1029/2004TC001627.

Consiglio Nazionale delle Ricerce (CNR)-Progetto Finalizzato Geodinamica (PFG) (1987). Neotectonic map of Italy, *Quaderni de La Ricerca Scientifica*, 114 pp.

Console, R., and M. Murru (2001). A simple and testable model for earthquake clustering, *J. Geophy. Res.* **106,** no. B5, 8699–8711.

Cramer, C. H. (2001). A seismic hazard uncertainty analysis for the New Madrid seismic zone, *Eng. Geol.* **62,** 251–266.

Cramer, C. H., M. D. Petersen, T. Cao, T. R. Toppozada, and M. Reichle (2000). A Time-dependent probabilistic seismic-hazard model for California, *Bull. Seismol. Soc. Am.* **90,** no. 1, 1–21.

Cramer, C. H., M. D. Petersen, and M. S. Reichle (1996) A Monte Carlo approach in estimating uncertainty for a seismic hazard assessment of Los Angeles, Ventura and Orange Counties, California, *Bull. Seismol. Soc. Am.* **86,** no. 6, 1681–1691.

D'Addezio, G., G. Masana, and D. Pantosti (2001). The Holocene paleoseismicity of the Aremogna-Cinque Miglia fault (central Italy), *J. Seism.* **5,** 181–205.

De Martini, P. M., N. A. Pino, G. Valensise, and S. Mazza (2003). Geodetic and seismologic evidence for slip variability along a blind normal fault in the Umbri-Marche 1997–1998 earthquakes (central Italy), *Geophys. J. Int.* **155,** 819–829.

Ellsworth, W. L. (1995). Characteristic earthquakes and long-term earthquake forecasts: implications of central California seismicity, in F. Y. Cheng and M. S. Sheu (Editors), *Urban Disaster Mitigation: the Role of Science and Technology*, Elsevier, 1–14.

Ellsworth, W. L., M. V. Matthews, R. M. Nadeau, S. P. Nishenko, P. A. Reasenberg, and R. W. Simpson (1999). A physically-based earthquake recurrence model for estimation of long-term earthquake probabilities, *U.S. Geol. Surv., Open-File Rept. 99–522*, 23 pp.

Elter, P., M. Grasso, M. Parotto, and L. Vezzani (2003). Structural setting of the Apennine-Maghrebian thrust belt, *Episodes* **26,** 205–211.

Erdik, M., M. Demircioglu, K. Sesetyan, E. Durukal, and B. Siyahi (2004). Earthquake hazard in Marmara region, Turkey, *Soil Dyn. Earthq. Eng.* **24,** 605–631.

Frankel, A. (1995). Mapping seismic hazard in the central and eastern United States, *Seism. Res. Lett.* **66,** no. 4, 8–21.

Frankel, A., C. Mueller, T. Barnhard, D. Perkins, E. V. Leyendecker, N. Dickman, S. Hanson, and M. Hooper (1996). National seismic hazard maps: documentation June 1996, *U.S. Geol. Surv. Open-File Rept. 96–532* 100 pp.

Frankel, A. D., M. D. Petersen, C. S. Muller, K. M. Haller, R. L. Wheeler, E. V. Leyendecker, R. L. Wesson, S. C. Harmsen, C. H. Cramer, D. M. Perkins, and K. S. Rukstales (2002). Documentation for the 2002 update of the national seismic hazard maps, *U.S. Geol. Surv. Open-File Rept. 02–420*, 33 pp.

Frapiccini, M., G. Monachesi, S. Del Mese, L. Giovani, A. Maramai, A. Tertulliani, and D. Molin (1997). Terremoto di Massa Martana del 12 maggio 1997: Rilevamento macrosismico preliminare dell'area maggiormente interessata, *Rapporto Protezione Civile*.

Galadini, F., and P. Galli (1999). The Holocene paleoearthquakes on the 1915 Avezzano earthquake faults (central Italy): implications for active tectonic in the central Apennines, *Tectonophysics* **308,** 143–170.

Galadini, F., and P. Galli (2000). Active tectonics in the central Apennines (Italy)-input data for seismic hazard assessment, *Nat. Haz.* **22,** 225–270.

Galadini, F., and P. Galli (2001). Archaeoseismology in Italy: case studies and implications on long-term seismicity, *J. Earthq. Eng.* **5,** 35–68.

Galadini, F., and P. Galli (2003). Paleoseismology of silent faults in the central Apennines (Italy): the Mt. Vettore and Laga Mts. faults, *Ann. Geophys.* **46,** 815–836.

Galadini, F., and P. Messina (1993). Characterization of the recent tectonics of the upper Sangro river valley (Abruzzi Apennine, central Italy), *Annali di Geofisica* **36,** no 1, 277–285.

Galadini, F., and P. Messina (2001). Plio-Quaternary changes of the normal fault architecture in the central Apennines (Italy), *Geodinamica Acta* **14,** 321–344.

Galadini, F., and P. Messina (2004). Early-middle Pleistocene eastward migration of the Abruzzi Apennine (central Italy) extensional domain, *J. Geodyn.* **37,** 57–81.

Galadini, F., P. Galli, I. Leschiutta, G. Monachesi, and M. Stucchi (1999). Active tectonics and seismicity in the area of the 1997 earthquake sequence in central Italy: a short review, *J. Seism.* **3,** 167–175.

Galadini, F., P. Galli, and M. Moro (2003) Paleoseismology of silent faults in the central Apennines (Italy): the Campo Imperatore fault (Gran Sasso Range fault system), *Ann. Geophys.* **46,** 793–813.

Galadini, F., C. Giraudi, and P. Messina (1998). Nuovi dati sulla tettonica tardopleistocenica dell'alta valle del Sangro: implicazioni sismotettoniche, *Il Quaternario* **11,** 347–356.

Galli, P., F. Galadini, M. Moro, and C. Giraudi (2002). New paleoseismological data from the Gran Sasso d'Italia area (central Apennines), *Geophys. Res. Lett.* **29,** no. 7, doi 10.1029/2001GL013292, 38.1–38.4.

Gasperini, P., F. Bernardini, G. Valensise, and E. Boschi (1999). Defining seismogenic sources from historical earthquake felt reports, *Bull. Seism. Soc. Am.* **89,** 94–110.

Giraudi, C., and M. Frezzotti (1995). Paleoseismicity in the Gran Sasso massif (Abruzzo, central Italy), *Quaternary Int.* **25,** 81–93.

Gori, S., F. Dramis, F. Galadini, and P. Messina (2007). The use of geomorphological markers in the footwall of active faults for kinematic evaluations: examples from the central Apennines, *Boll. Soc. Geol. It.* (Ital. J. Geosci.) **126,** no. 2, 365–374.

Gutenberg, B., and C. F. Richter (1949). Seismicity of the Earth and Associated Phenomena, Princeton University Press, Princeton.

Harmsen, S., and A. Frankel (2001). Geographic deaggregation of seismic hazard in the United States, *Bull. Seismol. Soc. Am.* **91,** no. 1, 7–24.

Kagan, Y. Y., and L. Knopoff (1987). Random stress and earthquake statistics; time dependence, *Geophys. J. R. Astr. Soc.* **88,** 723–731.

Kumamoto, T. (1999). Seismic hazard maps of Japan and computational differences in models and parameters, *Geograph. Rev. Japan*, Series B **72,** no. 2, 135–161.

Lindh, A. G. (1983). Preliminary assessment of long-term probabilities for large earthquakes along selected segments of the San Andreas fault system in California, *U.S. Geol. Surv. Open-File Rept. 83–63*, 15 pp.

Lombardi, A. M., A. Akinci, L. Malagnini, and C. H. Mueller (2005). Uncertainty analysis for seismic hazard in northern and central Italy, *Ann. Geophys.* **48,** 853–865.

Lundgren, P., and S. Stramondo (2002). Slip distribution of the 1997 Umbria-Marche earthquake sequence: joint inversion of GPS and synthetic aperture radar interferometry data, *J. Geophys. Res.* **107,** no. B11, 2316, doi 10.1029/2000JB000103.

Malagnini, L., and R. B. Herrman (2000). Ground-motion scaling in the region of the 1997 Umbria-Marche earthquake (Italy), *Bull. Seismol. Soc. Am.* **90,** 1041–1051.

Malagnini, L., A. Akinci, R. B. Herrmann, N. A. Pino, and L. Scognamiglio (2002). Characteristics of the ground-motion in northeastern Italy, *Bull. Seismol. Soc. Am.* **92,** 2186–2204.

Malagnini, L., R. B. Herrmann, and M. Di Bona (2000). Ground motion scaling in the Apennines (Italy), *Bull. Seismol. Soc. Am.* **90,** 1062–1081.

Matthews, M. V., W. L. Ellsworth, and P. A. Reasenberg (2002). A Brownian model for recurrent earthquakes, *Bull. Seismol. Soc. Am.* **92,** 2233–2250.

McGuire, R. K. (1995). Probabilistic seismic hazard and design earthquakes: closing the loop, *Bull. Seismol. Soc. Am.* **85,** no. 5, 1275–1284.

Meletti, M., E. Patacca, P. Scandone, and B. Figliuolo (1988). Il terremoto del 1456 e la sua interpretazione nel quadro sismotettonico dell'Appennino meridionale, in a c. di B. Figliuolo, Il terremoto del 1456, Istituto Italiano di Studi filosofici, *Storia e Scienza della Terra*, Vol. **2**, 71–163.

Messina, P., F. Galadini, P. Galli, and A. Sposato (2002). Quaternary basin evolution and present tectonic regime in the area of the 1997–98 Umbria-Marche seismic sequence (central Italy), *Geomorphology* **42,** 97–116.

Mirabella, F., and S. Pucci (2002). Integration of geological and geophysicaò data along a section crossing the region of the 1997–98 Umbria-Marche earthquakes (Italy), *Boll. Soc. Geol. It.* **1,** 891–900.

Molin, D., A. Rossi, A. Tertulliani, and V. e Verrubbi (2002). Studio della sismicità dell'alto Bacin dell'Aniene (Appennino centrale—Italia) e catalogo sismico di area, *Quaderni di Geofisica* **24,** 19–21.

Montaldo, V., E. Faccioli, G. Zonno, A. Akinci, and L. Malagnini (2005). Ground-motion predictive relationships for the reference seismic hazard map of Italy, *J. Seism.* **9,** 295–316.

Morasca, P., L. Malagnini, A. Akinci, D. Spallarossa, and R. B. Herrmann (2006). Ground-motion scaling in the western Alps, *J. Seism.* **10,** no. 3, 315–333.

Morgan, T. Page, and J. M. Carlson (2006). Methodologies for earthquake hazard assessment: model uncertainty and the WGCEP-2002 forecast, *Bull. Seismol. Soc. Am.* **96,** 1624–1633.

Moro, M., V. Bosi, F. Galadini, P. Galli, B. Giaccio, P. Messina, and A. Sposato (2002). Analisi paleosismologiche lungo la faglia del M. Marine (alta valle dell'Aterno): risultati preliminari, *Il Quaternario* **15,** 267–278.

Nishenko, S. P., and R. Buland (1987). A generic recurrence interval distribution for earthquake forecasting, **77,** 1382–1399.

Ogata, Y. (1999). Estimating the hazard of rupture using uncertain occurrence times of Paleoearthquakes, *J. Geophys. Res., B, Solid Earth Planets* **104,** no. 8, 17,995–18,014.

Olsen, K. B., A. Akinci, A. Rovelli, F. Marra, and L. Malagnini (2006). 3-D finite-difference modeling of earthquakes in the city of Rome, Italy, *Bull. Seismol. Soc. Am.* **96,** no. 1, 133–146.

Pace, B., L. Perruzza, G. Lavecchia, and P. Bancio (2006). Layered seismogenic source model and probabilistic seismic-hazard analyses in central Italy, *Bull. Seismol. Soc. Am.* **96,** 107–132.

Pantosti, D., G. D'Addezio, and F. R. Cinti (1996). Paleoseismicity of the Ovindoli-Pezza fault, central Apennines, Italy: a history including a large, previously unrecorded earthquake in the Middle Ages (860–1300 A.D.), *J. Geophys. Res.* **101,** 5937–5959.

Pantosti, D., D. P. Schwartz, and G. Valensise (1993). Paleoseismology along the 1980 surface rupture of the Irpinia fault: implications for earthquake recurrence in the southern Apennines, Italy, *J. Geophys. Res.* **98,** 6561–6577.

Papaioannou, C., and C. Papazachos (2000). Time-independent and time-dependent seismic hazard in Greece based on seismogenic sources, *Bull. Seismol. Soc. Am.* **90,** 22–33.

Peruzza, L., and B. Pace (2002). Sensitivity analysis for seismic source characteristics to probabilistic seismic hazard assessment in central Appennines (Abruzzo area), *Bollettino di Geofisica Teorica ed Applicata* **43,** 79–100.

Petersen, M. D., W. A. Bryant, C. H. Cramer, T. Cao, M. S. Reichle, A. D. Frankel, J. J. Lienkaemper, P. A. McCrory, and D. P. Schwartz (1996). Probabilistic seismic hazard assessment for the state of California, *U. S. Geol. Surv. Open-File Report OFR 96-0706*, 33 pp.

Petersen, M. D., T. Cao, K. W. Campbell, and A. D. Franke (2007). Time-independent and time-dependent seismic hazard assessment for the state of California: Uniform California $arthquake rupture forecast model 1.0, *Seism. Res. Lett.* **78,** no. 1 99–109.

Petersen, M. D., C. H. Cramer, M. S. Reichle, A. D. Frankel, and T. C. Hanks (2000). Discrepancy between earthquake rates implied by historic earthquakes and a consensus geologic source model for California, *Bull. Seismol. Soc. Am.* **90,** 1117–1132

Petersen, M. D., A. D. Frankel, S. C. Harmsen, C. S. Mueller, K. M. Haller, R. L. Wheeler, R. L. Wesson, Y. Zeng, O. S. Boyd, D. M. Perkins, N. Luco, E. H. Field, C. J. Wills, and K. S. Ruksatles (2008). Documentation for the 2008 update of the United States national seismic hazard maps, *U.S. Geol. Surv. Open-File Rept. 2008–1128*, 60 pp.

Pizzi, A., and S. Scisciani (2000). Methods for determining the Pleistocene-Holocene component of displacement on active faults reactivating pre-quaternary structures: examples from the central Apennines (Italy), *J. Geodyn.* **29,** 445–457.

Pizzi, A., F. Calamita, M. Coltorti, and P. Pieruccini (2002). Quaternary normal faults, intramontane basins and seismicity in the Umbria-Marche-Abruzzi Apennine ridge (Italy): contribution of neotectonic analysis to seismic hazard assessment, *Boll. Soc. Geol. It.*, Spec. Publ., **1,** 923–929.

Pucci, S., P. M. De Martini, D. Pantosti, and G. Valensise (2003). Geomorphology of the Gubbio basin (central Italy): understanding the active tectonics and earthquake potential, *Ann. Geophys.* **46,** 837–864.

Sabetta, F., and A. Pugliese (1996). Estimation of response spectra and simulation of non-stationary earthquake ground motions, *Bull. Seismol. Soc. Am.* **86,** 337–352.

Salvi, S., and A. Nardi (1995). The Ovindoli fault: a segment of a longer, active fault-zone in central Abruzzi (Italy), in *Perspectives in Paleoseismology*, L. Serva and D. B. Slemmons (Editors), *Bull. Assoc. Eng. Geol.*, Spec. Publ., Vol. **6**, 101–113.

Salvi, S., F. R. Cinti, L. Colini, G. D'Addezio, F. Doumaz, and E. Pettinelli (2003). Investigation of the active Celano-L'Aquila fault system, Abruzzi (central Appennines, Italy), with combined ground-penetrating radar and paleosismic trenching, *Geophys. J. Int.* **155,** 805–818.

Salvi, S., S. Stramondo, M. Cocco, M. Tesauro, I. Hunstad, M. Anzi dei, P. Brióle, P. Baldi, E. Sansosti, G. Fomaro, R. Lanari, F. Doumaz, A. Pesci, and A. Galvani (2000). Modeling coseismic displacements resulting from SAR interferometry and GPS measurements during the 1997 Umbria-Marche seismic sequence, *J. Seism.* **4,** 479–499.

Savage, J. C. (1991). Criticism of some forecasts of the national earthquake prediction council, *Bull. Seismol. Soc. Am.* **81,** 862–881.

Southern California Earthquake Center (SCEC) Phase II, (1994). Seismic hazards in southern California: probable earthquakes, 1994 to 2024 (Phase II), *SCEC Rept.*.

Scherbaum, F., J. Schmedes, and F. Cotton (2004). On the conversion of source-to-site, distance measures for extended earthquake source models, *Bull. Seismol. Soc. Am.* **94,** 1053–1069

Stucchi, M., A. Akinci, E. Faccioli, P. Gasperini, L. Malagnini, C. Meletti, V. Montaldo, and G. Valensise (2004). *Mappa di Pericolosità sismica del territorio Nazionale*, http://zonesismiche.mi.ingv.it/documenti/rapporto_conclusivo.pdf (in Italian).

Sykes, L. R., and S. P. Nishenko (1984). Probabilities of occurrence of large plate rupturing earthquakes for the San Andreas, San Jacinto, and Imperial faults, California, *J. Geophys. Res.* **89,** 5905–5927.

Tertulliani, A., and F. Riguzzi (1995). Earthquakes in Rome during the past one hundred years, *Ann. Geofis.* **38,** no. 5–6, 581–590.

Valensise, G. and D. Pantosti (Editors), (2001). Database of potential sources for earthquakes larger than *M* 5.5 in Italy, version 2.0, *Ann. Geofis.* **44,** 797–964.

Vittori, E., G. P. Cavinato, and E. Miccadei (1995). Active faulting along the northeastern edge of the Sulmona basin, central Apennines, Italy, in L. Serva and D. B. Slemmons (Editors), *Perspectives in Paleoseismology*, Ass. of Eng. Geologists, Spec. Publ., no. 6, 83–100.

Weichert, D. H. (1980). Estimation of the earthquake recurrence parameters for unequal observation periods for different magnitudes, *Bull. Seismol. Soc. Am.* **70,** 1337–1346.

Wells, D., and K. J. Coppersmith (1994). New empirical relationships among magnitude, rupture length, rupture width, rupture area and surface displacement, *Bull. Seismol. Soc. Am.* **84,** 974–1002.

Wessel, P., and W. H. F. Smith (1998). New, improved version of the Generic Mapping Tools released, in *EOS Trans.* American Geophysical Monograph **79,** 579.

Working Group on California Earthquake Probabilities (WGCEP) (1995). Seismic hazards in southern California: probable earthquakes, 1994 to 2024, *Bull. Seismol. Soc. Am.* **85,** 379–439.

Working Group on California Earthquake Probabilities (WGCEP) (2003). Earthquake Probabilities in the San Francisco Bay region: 2000 to 2030, *U.S. Geol. Surv. Circ. 1189*.

Working Group Catalogo Strumentale dei Terremoti Italiani (CSTI) (2001). Catalogo Strumentale dei Terremoti Italiani dal 1981 al 1996, vers. 1.0, Gruppo Nazionale per la Difesa dai Terremoti (Editors), Istituto Nazionale di Geofisica, Bologna, Italy.

Working Group Catalogo Parametrico dei Terremoti Italiani (CPTI) (2004). Catalogo Parametrico dei Terremoti Italiani, vers. 2004, Istituto Nazionale di Geofisica, Bologna, Italy.

Istituto Nazionale di Geofisica e Vulcanologia
Via di Vigna Murata 605
00143 Rome, Italy
akinci@ingv.it
pantosti@ingv.it
malagnini@ingv.it
(A.A., D.P., L.M.)

Istituto Nazionale di Geofisica e Vulcanologia
Sezione Milano-Pavia
20133 Milano, Italy
galadini@mi.ingv.it
(F.G.)

U. S. Geological Survey
MS 966, Box 25046
Denver, Colorado 80225
mpetersen@usgs.gov
perkins@usgs.gov
(M.P., D.P.)

Manuscript received 5 April 2008